SIMULATION OF TRANSITIONAL FLOW AND HEAT TRANSFER OVER TURBINE BLADES
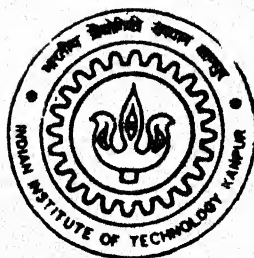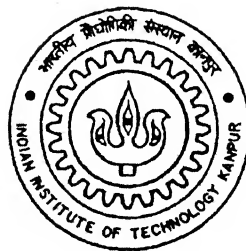
by

SANDIP DHAR

DEPARTMENT OF MECHANICAL ENGINEERING

INDIAN INSTITUTE OF TECHNOLOGY KANPUR

December, 1999

SIMULATION OF TRANSITIONAL FLOW AND HEAT TRANSFER OVER TURBINE BLADES

A Thesis Submitted
In Partial Fulfillment of the requirements
for the Degree of
Master of Technology

By
SANDIP DHAR

to the

Department of Mechanical Engineering

Indian Institute of Technology Kanpur

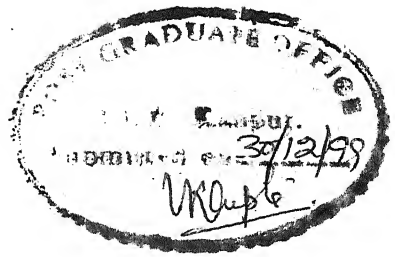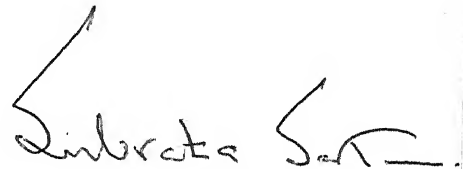**December 1999**

Dedicated to my beloved parents and elder sister

Certificate

It is to certify that the thesis entitled "SIMULATION OF TRANSITIONAL FLOW AND HEAT TRANSFER OVER TURBINE BLADES" by Mr. Sandip Dhar, has been carried out under my supervision. The contents of this thesis have not been submitted and will not be submitted to any other Institute or University for the award of any degree and diploma.

(Dr. Subrata Sarkar)

Assistant Professor,

Department of Mechanical Engineering,

Indian Institute of Technology,

Kanpur – 208016

29 December, 1999.

ACKNOWLEDGEMENT

CONTENTS

ABSTRACT

A classical way to improve the efficiency of a modern gas-turbine is to use increased inlet gas temperature. Thus, first few stages of turbine blades are exposed to high gas temperatures which are well above the metallurgical limit of the blade material used. Hence, turbine blade cooling is utmost needed to guarantee the life of an aero-engine. A prerequisite for the design of such turbine blades is a thorough knowledge of temperature distribution over the blade surface. Therefore, the prediction of flow and heat transfer around the blade is of great practical importance. A considerable amount of progress has been carried out in the development of flow solvers for turbomachinery applications over the last few decades. In spite of rapid advancement in the turbomachinery CFD field, some serious limitations of existing flow solvers have yet to be adequately resolved. Surely, the most profound of these is the lack of accuracy in predicting transitional flow, which is a critical issue for turbine blade heat transfer analysis.

Thrust of the present work is to implement a modified low-Reynolds-number k-ε turbulence model into a two-dimensional Navier-Stokes flow solver with Multigrid algorithm for the simulation of transitional flow and heat transfer through turbomachines. For the present calculation, the time-dependent, mass-averaged, two-dimensional, compressible Navier-Stokes equations are solved with additional two equations for turbulent-kinetic-energy (k) and dissipation rate (ε) by the four-stage Runge-Kutta method in finite volume formulations. Various acceleration techniques such as local time-

stepping ,variable coefficient implicit residual smoothing and a full Multigrid have been incorporated to accelerate the steady-state calculation. The turbulence model used here is the low-Reynolds-number version of the k-ε turbulence model due to Chien and also it has been modified with the Production-term-modification (PTM) technique of Schmidt and Patankar in order to improve both the qualitative and quantitative characteristics of the transition predictions. However, Schmidt and Patankar introduced the modification of production term within the framework of boundary layer type flow along a wall, where the marching technique can be applied to the resulting parabolic boundary layer equation. For the present analysis, the same modification is introduced into a general purpose two-dimensional, time-dependent full Navier-Stokes flow solver.

The solver has been used to predict the complex transitional flow and heat transfer over two turbine cascades for different exit Mach-numbers, Reynolds-numbers and free-stream turbulence levels. Comparisons of aerodynamics and convective heat transfer are made with experimental data. The overall prediction of transitional flow over turbine cascades for a widely varying flow conditions indicates that the low-Reynolds-number version of k-ε turbulence model due to Chien fails to predict the location of the onset of transition correctly, shows the tendency to predict the transition too early and over too short a distance. However, the heat transfer predicted over the laminar and fully turbulent part along with the surface Mach number distribution are compared well with the experimental observations. With the Production-term-modification in the turbulent-kinetic-energy equation, the shortcomings stated above are alleviated and the onset of transition as well as the length of transition are well resolved.

NOMENCLATURE

c	chord
c_x	axial chord
s	surface length
x, y, z	Cartesian co-ordinates
u	velocity component in x-direction
v	velocity component in y-direction
w	velocity component in z-direction
ρ	density
C	speed of sound
C_p	specific heat at constant pressure
C_v	specific heat at constant volume
e	total energy per unit mass
p	pressure
T	temperature
$\tau_{i,j}$	stress tensor
h	heat transfer co-efficient $= q_w/(T_{01}-T_w)$
k	turbulent kinetic energy
M	Mach number
Re	Reynolds Number

y^+	law-of-the wall coordinate
F, G	flux vectors
H	source terms vector
U	solution vector
P_r, P_{rt}	Prandtl Numbers
q_i	heat flux vectors
T_u	turbulence intensity
ε	dissipation rate
P_k	Production term
X	along cascade axial plane
Y	along blade to blade plane
γ	ratio of specific heat $= C_p/C_v$
u_τ	friction velocity $= \sqrt{\tau_w / \rho_w}$
Δ	small increment
$\delta_{i,j}$	Kronecker delta
μ, μ_t	molecular and turbulent viscosity
ν	kinematic viscosity
Ω	cell volume
Δt	time step
CFL	Courant-Friedrich-Lewis number

Subscripts

0	stagnation condition
1	inlet plane
2	exit plane
w	wall condition
t	turbulent
is	isentropic condition
i,j	logical cell indices in space
∞	free stream condition
h	fine grid level
2h, 4h	coarse grid level

Superscripts

n	time level
/	fluctuating quantity in density-weighted time averaging
—	time-averaged quantity
~	density-weighted time-averaged quantity

LIST OF FIGURES

CHAPTER - 1

INTRODUCTION

Modern aero engines may be characterized by their high power output, low specific fuel consumption, low weight, small size and high thrust to weight ratio. One of the major contributing factors towards this achievement is use of a high turbine entry gas-temperature and pressure-ratio. Moreover, turbomachinery flows are most complex in nature that encounter in practice including laminar, transitional and turbulent regions; stagnation flow; large pressure gradient and free stream turbulence; unsteady separated flow at the trailing edge; shock boundary layer interaction and so on. Thus, an improved understanding and prediction of flow and thermal fields is essential for designing the propulsion unit of a modern aero-engine. The level of accuracy for the simulation of such complex flows in turbomachinery demands an accurate and efficient flow solver with proper turbulence model that can predict transitional and separated regions.

With the advancement of computational-fluid-dynamics (CFD) in the last two decades, a considerable progress has been carried out in the development of Navier-Stokes flow solvers for turbomachinery applications. Most of the previous analyses, have given emphasis to obtain accurate aerodynamic behaviour of blades. The accurate heat transfer prediction in the turbine blade, which is also very important, is comparatively less attended. Thus a systematic analysis of flow and thermal field over turbine cascades for

widely varying flow conditions is seemed to be most desirable. As mentioned earlier, the lack of proper transition model for estimating the turbine blade heat transfer is a major and serious drawback for most of the modern flow solvers. It has been observed that a realistic simulation of the flow transition is of critical importance for turbomachinery applications, where the transition region is long in relation to the chord length of the blade. Success of computation, specially the heat transfer prediction depends on the choice of a transition model which can simulate the effects of free-stream-turbulence and pressure-gradient on the onset of transition. Two approaches are generally used to deal with this problem. The first is based on the use of an algebraic turbulence model along with an explicitly imposed model for transition. However, in principle this model is less reliable in the complex flow environment where multiple length scale exists and also where the transport of turbulent length scale is also important. The second approach is to use higher order models. Despite some deficiencies, low-Reynolds-number version of the k-ε models, which will provide the transport of length scales based on the local fluid and turbulent properties, are commonly used to simulate the flow transition.

The k-ε turbulence model incorporates the solution of two transport equations, one for the turbulent kinetic energy (k) and the other for the dissipation rate (ε). However, in their standard form these equations are not valid in regions very close to solid boundaries. To deal with this problem, several methods have been developed, one of which is to introduce special "low-Reynolds-number" functions into the equations for k and ε. About three decades ago, Jones and Launder [1972,1973] published their work on the introduction of these so-called Low-Reynolds-number functions into the framework of a

k-ε model. These functions modify or add to certain terms in the equations such that near wall damping effects are simulated. k-ε models that have been modified in this manner are commonly referred to as Low-Reynolds-number (LRN) k-ε models. At first, LRN k-ε models were applied to the calculation of flows in pipes, channels, and turbulent external boundary layers. Two of the notable successes of these models were the prediction of the correct Reynolds-number at which pipe flow becomes turbulent, and the relaminarisation of a turbulent boundary layer under a large accelerating pressure gradient. However, despite several shortcomings, these attractive features of LRN functions to mimic transition and relaminarisation, have tempted several researchers to apply LRN k-ε models in complex flow environment. The LRN functions are designed to simulate the proper viscous sub layer in a turbulent boundary layer, also damp out any turbulent production that would otherwise occur due to the influx of turbulent kinetic energy from the free-stream to the near wall region.

The main aim of the present investigation is to implement the low-Reynolds-number version of the k-ε turbulence model of Chien into a two-dimensional compressible Navier-Stokes flow solver with Multigrid algorithm for the simulation of transitional flow and heat transfer over turbine blades. The present work is based on a flow solver developed by my thesis supervisor, Prof. S. Sarkar and his former students, where the additional two equations for k and ε and its modified version are included to simulate the transitional flow and heat transfer. It should be noted that the LRN functions have almost all been formulated and applied only within the framework of boundary layer type flows along a wall, where marching technique can be applied to the resulting parabolic

equations. Schmidt and Patankar [1991] examined in details the capability of Low-Reynolds-number functions in two-equation models to simulate transitional flow using boundary layer equations. They observed some shortcomings involving the sensitivity of the starting location and profiles of turbulent-kinetic-energy and dissipation rate on the accuracy of the transition predictions over a range of turbulent intensities. They also observed that these functions have a tendency to predict transition earlier and over short a distance. To alleviate these shortcomings they introduced a modification in the production-term of the turbulent-kinetic-energy equation to control its growth rate. This approach has shown to overcome the shortcomings associated with the unmodified k-ε LRN models. However, the whole development was on boundary layer type equations where a space marching technique had been used to simulate the flow field. For the present analysis, the similar kind of modification is introduced in a general purpose flow solver where, the governing equations are unsteady, compressible Navier-Stokes equations and a time-dependent marching technique is used in finite volume formulations. It has been decided to use the LRN k-ε model of Chien to examine its capability to simulate transitional flow over transonic turbine blades. It is noted that the original Chien model fails to predict the proper location of the onset of transition, however, the laminar and the fully turbulent part are well-captured. The modified k-ε Chien model performs better in predicting the proper location and length of transition for a wide range of free-stream turbulence and Reynolds-numbers.

In short, the present investigation includes :

A systematic analysis of aerodynamics and convective blade surface heat transfer distribution over two different turbine cascades covering a wide range of Mach numbers, Reynolds numbers and free-stream turbulence levels.

A comparison of k-ε Chien model and Chien model modified with PTM technique in predicting transitional flow in turbine cascade is carried out.

CHAPTER – 2

LITERATURE REVIEW

In this chapter, a review of the literature pertaining to different two-equation turbulence models for the simulation of transitional and turbulent flow is presented. The major emphasis is given to the techniques for numerical implementation of different low-Reynolds-number k-ε turbulence models into advanced two-dimensional and three-dimensional Navier-Stokes solvers for turbomachinery flow analysis. Review of the published work on this field is also made to illustrate the state-of-the-art. For realistic prediction of transitional flow and heat transfer over turbine cascades one needs to solve the full Navier-Stokes equation with appropriate turbulence model.

One of the earliest works on two-equation turbulence models is due to Jones and Launder [1972] who introduced the so called "low-Reynolds-number" functions into the framework of a k-ε two-equation turbulence model. These functions modify or add to certain terms in the transport equations of k and ε such that near-wall damping effects are simulated. They applied their low-Reynolds-number two-equation turbulence model for the numerical predictions of various turbulent shear flows such as isothermal low Reynolds number pipe flows, wall boundary layer with stream-wise pressure gradient and wall injection; the predictions span both natural transition and relaminarisation.

Since that time, a variety of other models introducing similar types of functions has been suggested by other researchers.

Lam-Bremhorst [1981] modified the high Reynolds number form of the k-ε model and applied it to fully developed pipe flow for the prediction of wall turbulence. They established the validity of their model throughout the fully turbulent, semi-laminar and laminar regions of the flow. Chien [1982] introduced a low-Reynolds-number turbulence model for the prediction of channel and boundary layer flow. Rodi and Scheuerer[1986] used the low-Reynolds-number k-ε model of Lam-Bremhorst, standard k-ε model of Launder and Spalding, and one-equation model given by Norris and Reynolds to predict the boundary layer flows under adverse pressure gradient conditions. The one-equation model gives generally good results, the k-ε models reveals systematic discrepancies. They examined these shortcomings and employed a modification to the ε equation emphasizing the generation rate due to deceleration and got an improved prediction for both moderately and strongly decelerated flows. There exist different versions of low-Reynolds-number two-equation models, all are not mentioned.

Schmidt and Patankar [1991] presented a detailed analysis of the mechanism by which low-Reynolds-number (LRN) k-ε models simulate the transition process in external boundary layer flows subject to free-stream turbulence. They employed two representative models (Jones and Lanuder,1972 ; Lam and Bremhorst,1981) in a series of computational tests designed to evaluate the capability of these models to answer some specific practical questions concerning initial profile specification, starting location

sensitivity, and the relative accuracy of these models in predicting the correct location and length of the transition region over a range of free stream turbulent intensities. From their evaluation they concluded that although qualitative aspects of boundary layer transition under the influence of free stream turbulence were clearly predicted, without further development or modification, current LRN k-ε models were not particularly accurate. The problems described included difficulties associated with the sensitivity of the starting location, starting profile of k and ε as well as the tendency to predict transition too early and over too short a distance. So, they proposed a modification that limits the Production-term in the turbulent kinetic energy equation and is correlated to the free-stream turbulence level. This modification improves both qualitative and quantitative characteristics of the transition predictions and alleviates the difficulties of transition predictions by LRN k-ε models in external boundary layer flows.

Ridha Abid [1993] conducted an evaluation of the capabilities and limitations of four low-Reynolds-number two-equation turbulence models for predicting bypass transition on a flat plate. He tested the ability of these models to reproduce the effect of free-stream turbulence on transition. He clarified that k-ε models are capable of predicting the qualitative aspects of transition, and the start and end of transition depend on the damping functions used in the low-Reynolds-number versions of the k-ε turbulence models. The transition predictions were found to be sensitive to the initial profiles of k and ε. The transition length was consistently under-predicted.

So far, the applications of low-Reynolds-number k-ε turbulence models discussed here were restricted to the boundary layer flows along a wall, where marching techniques can be applied to the resulting parabolic boundary layer equations. The implementation of these low-Reynolds-number k-ε turbulence models in a general purpose Navier-Stokes solver for complex flows such as flow through turbomachinery was carried out recently.

G.A Gerolymos [1990], one of the pioneer researchers developed a numerical method for solving the compressible Navier-Stokes equations using a low-Reynolds-number two-equation k-ε model of Launder-Sharma. He applied his solver to the numerical predictions of shock wave / turbulent boundary layer interaction in a symmetric channel on both walls of which interchangeable half profiles were mounted. He also applied his solver to the fully turbulent flow produced in a non-symmetric channel where a half profile was mounted on the lower wall of the wind tunnel test section. He used an explicit, implicitly smoothed, multiple-grid algorithm and local time-stepping to accelerate the convergence. The implementation of the k-ε model was successful in not altering the time steps used for the integration of the Navier-Stokes equations, when compared with algebraic turbulence closures. The use of implicit residual smoothing on every grid significantly improves the convergence rate. He concluded that it would be possible to use k-ε closure in efficient time-marching algorithm, without degrading neither stability, nor convergence rate characteristics.

Kunz and Lakshminarayana [1992a] developed a fully explicit two-dimensional flow solver based on a four stage Runge-Kutta scheme with low-Reynolds-number

9

compressible form of the k-ε model due to Chien to predict turbulent viscous flow through turbomachinery cascades. They used anisotropic scaling of artificial dissipation terms and locally varying time step based on hyperbolic and parabolic stability criteria. They applied their solver to predict viscous flow through a supersonic and a low-subsonic compressor cascade. Their code was found to be capable of predicting steady two dimensional turbulent flow through cascade over a wide range of Mach numbers in reasonable computation times. They concluded that a fully explicit treatment of the turbulent transport equations would be possible. Overall cascade performance parameters were well-predicted for the supersonic cascade but, for low subsonic cascade the prediction was not good due to flow field unsteadiness. Kunz and Lakshminarayana [1992b] extended their fully explicit two-dimensional flow solver to the three-dimensional and successfully applied to complex internal flow calculations in turbomachinery. From their analysis, it was found that the technique provides accurate and efficient method for simulation of complex turbulent secondary flows in turbomachinery.

Turner and Jennions [1993] developed an explicit Navier-Stokes solver with an implicit k-ε model in a coupled way. They applied the resulting code to the solution of flow in a transonic fan rotor. They used five different turbulence models such as the standard Baldwin-Lomax model both with and without wall functions, the Baldwin-Lomax model with modified constants and wall functions, a standard k-ε model, and an extended k-ε model, which accounts for multiple time scales by adding an extra term to the dissipation equation. The numerical scheme for solving the k-ε equations was based on an implicit

staggered grid method for solving convection diffusion equations. Coupling the implicit k-ε equations with the explicit Navier-Stokes solver was found to be successful. The flow rate for the k-ε equation was closer to experiment than the Baldwin-Lomax solutions and the extended k-ε model performed better than the standard k-ε model

Biswas and Fukuyama [1994] analyzed several well-known low-Reynolds-number versions of the k-ε models (Launder-Sharma, Lam-Bremhorst, Nagano-Tagawa, Kasagi-Sikasono) for numerical predictions of laminar to turbulent transitional flows and near-wall turbulent flows. After examining the problems associated with the modeling of low-Reynolds-number wall damping functions used in these models, they proposed an improved version of the k-ε model by defining the wall damping factors as a function of turbulent Reynolds number. They applied this new model to the prediction of transitional boundary layers influenced by the free stream turbulence, pressure gradient, and external heat transfer distribution on the gas turbine rotor and stator blade under different inlet Reynolds number and free-stream conditions. Their model, despite some discrepancies showed improved predictions of transitional boundary layer on a flat plate and heat transfer distribution on the turbine blade.

Sarkar [1996] used the low-Reynolds-number version of the two-equation model of Chien in an explicit, time-split, cell-centered finite-volume scheme of MacCormack for the simulation of transitional flow and heat transfer over transonic turbine cascades. He also compared the performance of LRN Chien model with the algebraic Baldwin-Lomax model with an explicitly imposed model for transition in predicting the transitional flow

and heat transfer over transonic turbine cascades for a widely varying flow conditions. The modified Baldwin-Lomax model performed well when the flow was mainly governed by the onset of laminar-turbulent transition. The effects of free stream turbulence and pressure gradient on the transition process and the transition length was better resolved by the LRN Chien model. However, there were discrepancies with experimental observations and predictions for high exit Reynolds number.

Luo and Lakshminarayana [1997] investigated the boundary layer development and convective heat transfer on transonic turbine nozzle vanes using a compressible Navier-Stokes solver with three low-Reynolds-number k-ε models. They examined the effect of blade surface pressure gradient, free-stream turbulence level and Reynolds-number on the blade boundary layer development, and onset of transition . They used Lam-Bremhorst, Chien and Fan-Lakshminarayana-Barnett k-ε models. They studied two modes of transition, bypass transition and separation induced transition comparatively. The Navier-Stokes predictions with these low-Reynolds-number k-ε models, despite some discrepancies captured the location of separation induced transition well. The Lam-Bremhorst k-ε model provided relatively better predictions of the transition and the heat transfer than the other two models. Chien LRN k-ε model predicted a premature transition in their investigation.

Sarkar and Bose [1995] used different low-Reynolds-number versions of two-equation turbulence models in predicting the flow field and heat transfer phenomena created by the jet-cross flow interactions for film cooling applications. They compared the performance

of the LRN k-ε Chien model with other LRN models such as Lam-Bremhorst k-ε model ,
Wilcox k-ω model and algebraic Baldwin-Lomax model and also a relaxation eddy
viscosity model. The time-dependent, density-weighted Navier-Stokes equations coupled
with the compressible form of two-equation models were solved based on an explicit
finite volume formulation in their work. Considering both the predicted surface
temperature distributions and the relaxation behaviour of the velocity, low-Reynolds-
number versions of the k-ε models seemed to perform better compared to others.

Michelassi, Martelli, Denos, Arts, Sieverding [1999] applied the two-equation turbulence
model for the computation of unsteady heat transfer in Stator-Rotor interaction in a
transonic turbine stage. They used Wilcox's k-ω model coupled to a transition model
based on integral parameters and an extra transport equation. They carried out an analysis
of the transonic turbine stage with stator trailing edge coolant injection to compute the
unsteady pressure and heat transfer distribution on the rotor blade under variable
operating conditions.

The present review of literature reveals that a significant progress has been made in the
development of low-Reynolds-number forms of two-equation turbulence models.
Applications of these models on complex turbomachinery flows illustrate that the models
are successful to predict fully turbulent flows with certain discrepancies acceptable for
engineering applications. However, there exists a lot of uncertainties in predicting
transitional flows even with engineering stand-point. It appears to the investigator to
modify the low-Reynolds-number version of two-equation turbulence model in a

framework of Navier-Stokes solver and apply that for simulation of flows of practical interest and complexity that is flows through turbine cascades.

CHAPTER – 3

GOVERNING EQUATIONS

3.1 Introduction

The main objective of the present study is to numerically simulate the complex two-dimensional transitional flow and heat transfer in turbomachinery blade passage. Also, the present study examines the ability of low-Reynolds-number two-equation turbulence model in estimating the onset of transition and heat transfer in turbine blades. In this chapter, the mass averaged two-dimensional Navier-Stokes equations and transport equations for two-equation turbulence model are presented.

In the present analysis, density-weighted time-averaging of Favre [1965] is used. The density-weighted averaging leads to a simpler form of the governing equations with terms that are amenable to physical interpretation. It should be noted that density-weighted time-averaging is used for velocity components, temperature, turbulent kinetic energy, and dissipation rate, whereas the conventional time averaging is used for pressure, density, stress tensor and heat flux vector. It should be emphasized here that the main flow solver was developed by Sarkar [1999]. The contribution of the present investigation is to add two additional equations for k and ε for turbulent flows.

3.2 Mean flow Equations

The time-dependent, mass-averaged, two-dimensional compressible Navier-Stokes equations can be expressed in "conservative form" as

$$\frac{\partial U}{\partial t} + \frac{\partial F}{\partial x} + \frac{\partial G}{\partial y} = H \tag{1}$$

where,

$$U = \begin{bmatrix} \bar{\rho} \\ \bar{\rho}\tilde{u} \\ \bar{\rho}\tilde{v} \\ \bar{\rho}\tilde{e} \end{bmatrix} \qquad\qquad F = \begin{bmatrix} \bar{\rho}\tilde{u} \\ \bar{\rho}\tilde{u}^2 + \bar{p} - \bar{\tau}_{xx} \\ \bar{\rho}\tilde{u}\tilde{v} - \bar{\tau}_{xy} \\ (\bar{\rho}\tilde{e} + \bar{p} - \bar{\tau}_{xx})\tilde{u} - \bar{\tau}_{xy}\tilde{v} + \bar{q}_x \end{bmatrix}$$

$$G = \begin{bmatrix} \bar{\rho}\tilde{v} \\ \bar{\rho}\tilde{u}\tilde{v} - \bar{\tau}_{yx} \\ \bar{\rho}\tilde{v}^2 + \bar{p} - \bar{\tau}_{yy} \\ (\bar{\rho}\tilde{e} + \bar{p} - \bar{\tau}_{yy})\tilde{v} - \bar{\tau}_{yx}\tilde{u} + \bar{q}_y \end{bmatrix} \quad \text{and} \quad H = \begin{bmatrix} 0 \\ 0 \\ 0 \\ 0 \end{bmatrix} \tag{2}$$

are state vector, convective flux vectors in the x and y directions, and source terms vector, respectively. The total stress tensor and the heat flux vector are given in Cartesian coordinates as

$$\bar{\tau}_{ij} = \mu\left[\left(\frac{\partial \tilde{u}_i}{\partial x_j} + \frac{\partial \tilde{u}_j}{\partial x_i}\right) - \frac{2}{3}\delta_{ij}\frac{\partial \tilde{u}_k}{\partial x_k}\right] + \bar{\tau}_{t_{ij}}$$

16

and
$$\bar{q}_i = -\frac{\mu c_p}{Pr}\frac{\partial \widetilde{T}}{\partial x_i} + \bar{q}_{t_i} \qquad (3)$$

In the present study, the laminar viscosity coefficient μ is assumed to be a function of temperature only, and is evaluated following the Sutherland 's law which is given by,

$$\mu = C_1 \frac{(T)^{3/2}}{T + C_2}$$;where C_1 and C_2 are constants for a given gas. For air at moderate temperatures, $C_1 = 1.458 \times 10^{-6}$ kg/(ms$\sqrt{^\circ K}$) and $C_2 = 110.4^\circ K$. The perfect gas equation of state $\bar{p} = \bar{\rho}R\widetilde{T}$, is considered to be applicable. In preceding expressions, $\bar{\tau}_{t_{ij}}$ and $\bar{q}_{t_i}$ represent the turbulent stress tensor and heat flux vector, which are to be evaluated for the closure of equation (1). To accomplish this, a low-Reynolds-number two-equation turbulence model is used specifying a turbulent Prandtl number $Pr_t = 0.9$.

3.3 Turbulence Model

The turbulence model used here is basically the low-Reynolds-number version of the two-equation turbulence model due to Chien and later it has been modified with the Production-Term-Modification (PTM) technique of Schmidt and Patankar [1991].

Two-equation model :

By definition, a two-equation model requires solution of two-transport equations in addition to those expressing conservation of mass, momentum and energy. Incorporating an eddy viscosity formulation, the turbulence stress tensor and heat flux vector are given by

$$\overline{\tau}_{t_{ij}} = -\overline{\rho\widetilde{u}_i'\widetilde{u}_j'} = \mu_t\left[\left(\frac{\partial\widetilde{u}_i}{\partial x_j}+\frac{\partial\widetilde{u}_j}{\partial x_i}\right)-\frac{2}{3}\delta_{ij}\frac{\partial\widetilde{u}_k}{\partial x_k}\right]-\frac{2}{3}\delta_{ij}\overline{\rho}k$$

and $\quad \overline{q}_{t_i} = -\dfrac{\mu_t c_p}{Pr_t}\dfrac{\partial\widetilde{T}}{\partial x_i}$ (4)

k-ε turbulence model :

For the k-ε model the eddy viscosity is

$$\mu_t = c_\mu f_\mu \frac{\overline{\rho}k^2}{\varepsilon}$$ (5)

where k is the turbulent kinetic energy and ε is the dissipation rate. These turbulent quantities are obtained from their transport equations, which can be expressed in the same form as Eq. (1), where the variable vectors become

$$U = \begin{bmatrix} \bar{\rho}k \\ \bar{\rho}\varepsilon \end{bmatrix} \qquad\qquad F = \begin{bmatrix} \bar{\rho}\tilde{u}k - \left(\mu + \dfrac{\mu_t}{\sigma_k}\right)\dfrac{\partial k}{\partial x} \\[2ex] \bar{\rho}\tilde{u}\varepsilon - \left(\mu + \dfrac{\mu_t}{\sigma_\varepsilon}\right)\dfrac{\partial \varepsilon}{\partial x} \end{bmatrix}$$

$$(6)$$

$$G = \begin{bmatrix} \bar{\rho}\tilde{v}k - \left(\mu + \dfrac{\mu_t}{\sigma_k}\right)\dfrac{\partial k}{\partial y} \\[2ex] \bar{\rho}\tilde{v}\varepsilon - \left(\mu + \dfrac{\mu_t}{\sigma_\varepsilon}\right)\dfrac{\partial \varepsilon}{\partial y} \end{bmatrix} \qquad H = \begin{bmatrix} P_k - \bar{\rho}\varepsilon + D \\[2ex] c_{\varepsilon 1}f_{\varepsilon 1}P_k\dfrac{\varepsilon}{k} - c_{\varepsilon 2}f_{\varepsilon 2}\dfrac{\bar{\rho}\varepsilon^2}{k} + E_\varepsilon \end{bmatrix}$$

The production term P_k is expressed in Cartesian coordinates as

$$P_k = \bar{\tau}_{t_{xx}}\frac{\partial \tilde{u}}{\partial x} + \bar{\tau}_{t_{xy}}\left(\frac{\partial \tilde{u}}{\partial y} + \frac{\partial \tilde{v}}{\partial x}\right) + \bar{\tau}_{t_{yy}}\frac{\partial \tilde{v}}{\partial y} \qquad (7)$$

Here, $c_\mu, c_{\varepsilon 1}, c_{\varepsilon 2}, \sigma_k,$ and σ_ε are the model constants. $f_\mu, f_{\varepsilon 1}$, and $f_{\varepsilon 2}$ are the damping functions used to simulate the low-Reynolds number effects. The terms D and E_ε model the near-wall effects. The damping functions depend on one or more of the following two dimensionless parameters :

$$Re_T = \frac{\bar{\rho}k^2}{\mu\varepsilon} \qquad\qquad\qquad y^+ = \frac{\bar{\rho}u_\tau y}{\mu}$$

The damping functions, closure coefficients, and surface boundary conditions for the low-Reynolds-number version of the k-ε turbulence model due to Chien considered in the present analysis are as follows :

$$f_\mu = 1 - \exp\left(-0.0115 y^+\right)$$

$$f_{\varepsilon 1} = 1.0$$

$$f_{\varepsilon 2} = 1 - \left(\frac{2}{9}\right) \exp\left(-\frac{Re_T^2}{36}\right) \tag{8}$$

$$D = \frac{-2\mu k}{y^2}$$

$$E_\varepsilon = -\left(\frac{2\mu\varepsilon}{y^2}\right) \exp\left(-0.5 y^+\right)$$

$$c_\mu = 0.09 \qquad c_{\varepsilon 1} = 1.35 \qquad c_{\varepsilon 2} = 1.80 \qquad \sigma_k = 1.0 \qquad \sigma_\varepsilon = 1.3$$

$$k = 0 \quad \text{and} \quad \varepsilon = 0 \quad \text{at} \quad y = 0$$

It should be noted that although the k-ε equations have been cast in compressible form, the modeling assumptions invoked here are essentially those for incompressible flow. The terms containing density fluctuation and pressure diffusion are neglected. In the present work, these two additional mass-averaged transport equations are solved in coupled with the mean-flow equations.

It has been decided to use low-Reynolds-number version of two-equation model due to Chien to simulate the transitional flow over transonic turbine cascade with the hope that LRN function mimic some aspects of the physical behaviour associated with flow stability. The Chien model is introduced in a framework of the general purpose Navier-Stokes solver written in the finite volume formulation. After series of numerical experimentation, it has been observed that although the LRN two-equation models predict some aspects of transitional flow over turbine blades, there exist significant discrepancies with the experimental observations. Schmidt and Patankar [1991] described the similar kind of behaviour with LRN two-equation models while predicting transitional flow over a flat plate even with boundary layer equations. The observation is, the LRN k-ε models have a tendency to predict transition much earlier than the experimental observation and over short a distance. Thus, it seems to the author to invoke some corrections or modifications to the existing LRN two-equation turbulence models to mimic in a more realistic way the physical behaviour of instability associated with transitional flow as a function of free-stream turbulence and pressure gradient.

At this stage, it is necessary to explain how LRN k-ε models simulate transitional flow. It is explained by Schmidt and Patankar [1991].

LRN k-ε models to Simulate Transition:

The process of transition as predicted by LRN k-ε models is explained with the aid of figure-3.1, which shows the typical development of the turbulent-kinetic-energy profiles
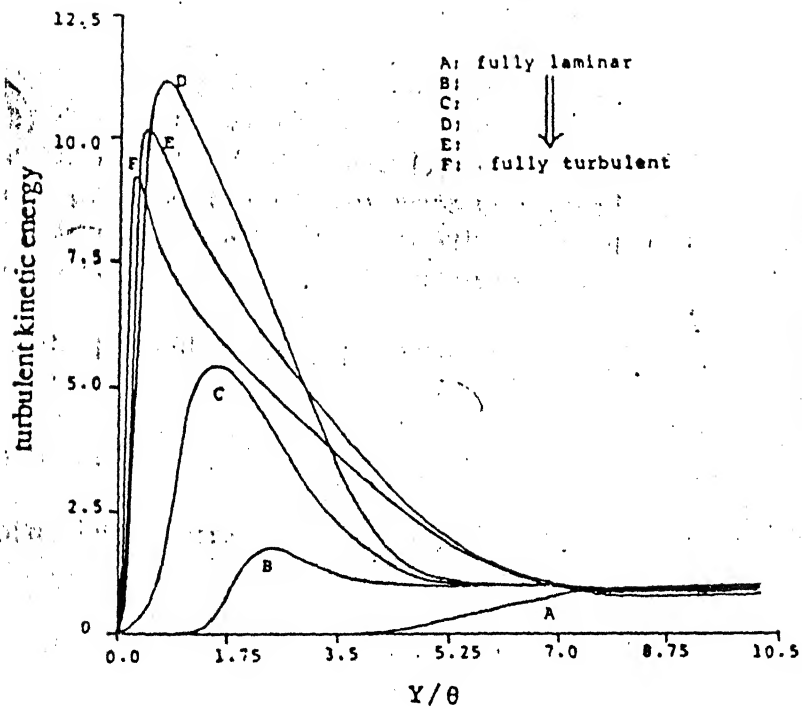
Fig 3.1 Development of the turbulent kinetic energy profiles as simulated by Schmidt and Patankar [1991].

as the simulated flow proceeds from a laminar to a turbulent state. Initially, the turbulent-kinetic-energy is monotonic, increasing slowly from zero at the wall to the free stream turbulent kinetic energy level (k_e) at the boundary. As the calculation marches downstream (when the boundary layer type of equation would be used), the turbulent-kinetic-energy from the free stream is convected and diffused in to the boundary layer. As this continues, the production-term in the two-equation model starts to become significant. This in turn, enhances the local value of k and thus μ_t. This process feeds on itself, causing a rapid increase in k. It should be noted that a large overshoot occurs initially, then slowly decays until a relatively stable state due to the LRN functions is achieved. Moreover, the LRN functions, designed to simulate the proper viscous sublayer in a turbulent boundary layer, also damp out any turbulent-production that would otherwise occur due to the influx of turbulent kinetic energy from the free stream region to the near-wall region.

Thus, the process of transition is controlled by the convection and diffusion of k into the boundary layer from the free stream, and also its interaction with the non-linear source terms in the k and ε equations. The final stages of this process are manifested very clearly by a relatively sharp increase in the skin-friction and also in heat transfer.

As already explained, LRN k-ε turbulence models even when applied to predict transition over a flat plate using boundary layer type equation exhibit the flowing shortcomings :

1. The sensitivity of the prediction depends on the location and specification of initial profiles of k and ε.

2. Tendency to predict transition early and over short a distance.

To alleviate these difficulties, Schmidt and Patankar proposed some modification to limit the growth-rate of Production-term in the LRN two-equation models to simulate transition in a more realistic manner. The modification introduced by them is explained below.

A modification to the Production-term :

In the k-ε models, the Production-term (P_k) in the k equation is the only term that can drive the near-wall profile of k to values above that of the free-stream. Thus, this term is a logical place for stability related information to be applied, and also where the transition rate might be controlled. So, a modification to limit the growth-rate of Production-term was introduced . Its form leaves the fully turbulent calculations undisturbed, but introduced a maximum rate at which P_k can increase in time. The time scale used was simply related to the local velocity.

The modification is given by,

$$\frac{dP_{k\,max}}{dt} = A * P_k + B \tag{9}$$

where, A and B, are empirical parameters, and the subscript "max" denotes the maximum allowable value . The dependence of the linear term on P_k was arbitrarily suggested by analogy with reaction-rate theory, but also found to yield acceptable results. The two parameters, A and B were directly related to the start and end of transition; the values of which were arrived from the correlation of transition expressed by Abu-Ghannam and Shaw [1980] from their experimental observations. As a means of incorporating some stability information, they proposed to eliminate P_k from the k equation below some critical momentum thickness Reynolds number $\left(Re_{\theta,c}\right)$.

The numerical implementation of their modification in the boundary layer code was as follows :

x = stream-wise location at the current point in the calculation

dx = step size in stream-wise direction

PE(j,x) = computed positive source-term in the ε equation of the jth control volume and at stream-wise location x.

PK(j,x) = computed positive source-term in the k-equation for the jth control volume and at stream-wise location x.

U_j = local stream-wise velocity at the jth control volume.

To compute the value of the value of PK(j,x+dx) to be used over the next step in the solution, the following (written in pseudo-fortran) were implemented.

$$PE(j,x+dx) = \frac{\varepsilon}{k} C_1 f_1 \mu_t \left(\frac{\partial U}{\partial y}\right)^2$$

$$\Delta P_{k,max} = \left(A * PK(j,x) + B\right)\frac{dx}{U_j}$$

If $Re_\theta \langle Re_{\theta,c}$ then

$$PK(j,x+dx) = 0$$

else

$$PK(j,x+dx) = PK(j,x) + min\left[\mu_t\left(\frac{\partial U}{\partial y}\right)^2 - PK(j,x), \Delta P_{k,max}\right]$$

endif

In their case, the whole development was on boundary layer type parabolic equations

where a space marching technique had been used to simulate the flow field over a flat

plate. For the present analysis, the similar kind of modification is introduced in a general

purpose flow solver, where, the governing equations are unsteady, compressible Navier-

Stokes equations and a time-dependent marching technique is used in finite volume

formulations. In the process of implementation of modification to the Production-term,

Schmidt and Patankar replaced the time scale simply by local velocity as $\frac{dx}{U_j}$, since the

equation was boundary layer type. In contrary, while using the same modification, in a

time-dependent treatment, the term $\frac{dP_{k\,max}}{dt}$ can be evaluated using the local time step.

However, numerical experimentation suggests to include some upstream effects by a

relaxation factor. The implementation of the modification in a full Navier-Stokes solver as carried out in the present investigation is explained below.

The production of turbulent-kinetic-energy at current time level for a particular cell (i,j), denoted by the variable PROD, is evaluated as

$$PROD = 0.7 * P_{k_{i-1,j}}^{n-1} + 0.3 * P_{k_{i,j}}^{n}$$

where, $P_{k_{i,j}}^{n}$ is the Production-term at the nth time level for the (i,j)th cell.

Using the above expression, the upstream effect is taken to estimate the Production-term at the current time level.

The following steps are :

$$\text{if } Re_\theta \langle Re_{\theta,c} \text{ then}$$

$$P_{k_{i,j}}^{n} = PROD$$

else

$$\Delta P_{k,max} = (A * PROD + B) * DTL(i,j)$$

where, DTL(i,j) is the local time step.

$$\Delta P_{k,max} = max[\Delta P_{k,max}, 0.0]$$

$$P_{k_{i,j}}^{n} = PROD + min[(P_{k_{i,j}}^{n} - PROD), \Delta P_{k,max}]$$

endif

Thus, the above modification limits the growth rate of Production-term after the momentum thickness Reynolds number reaches the critical value. This growth-rate is correlated to the experimental observations by the transition parameters A and B. The values of the constants A and B are found out by numerical experimentation in accord with the correlation of Abu-Ghannam and Shaw [1980] and their values are as follows :

$$\overline{A} = -0.5654 \times 10^{-6} \quad \text{and} \quad \overline{B} = 7.0632 \times 10^{-12} \quad \text{for 4\% turbulence-intensity}$$

$$\overline{A} = -4.1411 \times 10^{-6} \quad \text{and} \quad \overline{B} = 15.2813 \times 10^{-12} \quad \text{for 6\% turbulence-intensity}$$

where, $\overline{A}$ and $\overline{B}$ are the non-dimensional values of transition parameters A and B respectively. $\overline{A}$ and $\overline{B}$ are given by

$$\overline{A} = \frac{A\mu}{\rho U^2} \qquad \text{and} \qquad \overline{B} = \frac{B\mu^2}{\rho^3 U^6}$$

CHAPTER - 4

NUMERICAL SCHEME

The time-dependent, mass-averaged, two-dimensional compressible Navier-Stokes equations are solved with the low-Reynolds-number version of the k-ε turbulence model due to Chien simultaneously. The integration of the previously mentioned six equations (mass, momentum, energy, transport equations for k and ε) in time is based on an explicit four-stage Runge-Kutta scheme in the finite formulation. Local time-stepping, variable coefficient implicit residual smoothing and a full multigrid method have been implemented to accelerate the steady-state calculations.

The computational domain is divided into quadrilateral cells, fixed in time, and for each cell the governing equations are written in the integral form as,

$$\frac{\partial}{\partial t} \int_{\Omega} \overline{U} d\Omega + \int_{s} \overline{Q}.d\overline{S} = \int_{\Omega} H d\Omega$$

where, Ω denotes the volume of the control volume being considered, $d\overline{S}$ is the surface normal, $\overline{Q} = \left(\overline{F}, \overline{G}\right)$, the flux vector, U is the state vector and H is the source term.

A simple discretised form of the above equation for a discrete cell $\left(i, j\right)$, is given by,

$$\frac{d}{dt}\left(\Omega_{i,j} U_{i,j}\right) + Q(U)_{i,j} = H_{i,j}\Omega_{i,j}$$

where, $\Omega_{i,j}$ is the volume of the discrete cell and $Q(U)_{i,j}$ are finite volume approximations for the net convective and diffusive fluxes out of the discrete cell and $H_{i,j}$ is the source term at the center of the discrete cell.

For the viscous flows, dissipative properties are present because of diffusive terms; however, due to nonlinear effects the physical dissipation may not be sufficient to guarantee stability, especially in the case of the highly stretched meshes generally used to resolve the steep gradients in shear layers. Thus, to maintain stability and robustness of the numerical procedure, artificial dissipation is also included in viscous calculations. It is given by,

$$\frac{d}{dt}\left(\Omega_{i,j} U_{i,j}\right) + Q(U)_{i,j} - D(U)_{i,j} = H_{i,j}\Omega_{i,j} \tag{1}$$

where, $D(U)_{i,j}$ is the artificial dissipation term of the discrete cell.

Artificial Dissipation :

The artificial dissipation model considered here, is basically the one developed by Jameson [1981]. This is a blending of second- and fourth-order differences of flow variables. The original dissipation model is extended and known as non-isotropic

dissipation model to include the effect of cell-aspect ratio particularly near the wall. The quantity $D(U)$ is defined as,

$$D(U) = \left(D_\xi^2 - D_\xi^4 + D_\eta^2 - D_\eta^4\right)U$$

where, (ξ, η) are arbitrary curvilinear co-ordinates,

$$D_\xi^2 U = \nabla_\xi \left(\lambda_{i+1/2,j}.\varepsilon^2{}_{i+1/2,j}\right)\Delta_\xi U_{i,j}$$

$$D_\xi^4 U = \nabla_\xi \left(\lambda_{i+1/2,j}.\varepsilon^4{}_{i+1/2,j}\right)\Delta_\xi \nabla_\xi \Delta_\xi U_{i,j}$$

and i, j are indices (for a cell center) associated with the ξ and η directions. The operators Δ_ξ, ∇_ξ are forward and backward difference operators in the ξ direction. The variable scaling factor is defined as,

$$\lambda_{i+1/2,j} = \frac{1}{2}\left[\left(\overline{\lambda}_\xi\right)_{i,j} + \left(\overline{\lambda}_\xi\right)_{i+1,j}\right]$$

$$\left(\overline{\lambda}_\xi\right)_{i,j} = \phi_{i,j}(r)\left(\lambda_\xi\right)_{i,j}$$

$$\phi_{i,j}(r) = 1 + r^\zeta{}_{i,j}$$

Here, $r = \dfrac{\lambda_\eta}{\lambda_\xi}$ with λ_η and λ_ξ denoting the scaled spectral radii of the flux Jacobian matrices of $\overline{Q}.\overline{S}_\xi$ and $\overline{Q}.\overline{S}_\eta$ associated with the ξ and η directions. The exponent ζ is generally defined by $2/3 \leq \zeta \leq 1$. The spectral radii for ξ and η directions are given by

$$\lambda_\xi = \overline{q}.\overline{S}_\xi + c\left|\overline{S}_\xi\right|$$

$$\lambda_\eta = \overline{q}.\overline{S}_\eta + c\left|\overline{S}_\eta\right|$$

where, $\bar{S}_\xi$ and $\bar{S}_\eta$ are the cell surface normal vector along each grid line direction, $\bar{q} = (u, v)$ is the velocity vector and c is the speed of sound. The coefficients ε^2 and ε^4 use the pressure as a sensor for shocks and stagnation points, and they are defined as

$$\varepsilon^2{}_{i+1/2,j} = k^2 \max\left(v_{i-1,j}, v_{i,j}, v_{i+1,j}, v_{i+2,j}\right)$$

$$v_{i,j} = \frac{\left|P_{i-1,j} - 2P_{i,j} + P_{i+1,j}\right|}{\left|P_{i-1,j} + 2P_{i,j} + P_{i+1,j}\right|}$$

$$\varepsilon^4{}_{i+1/2,j} = \max\left[0, \left(k^4 - \varepsilon^2{}_{i+1/2,j}\right)\right]$$

where, the typical values for the constants $\bar{k}^2$ and k^4 are $1/4$ and $1/64$ respectively.

For the normal direction (η), the dissipation contributions are defined in a similar way, except

$$\left(\bar{\lambda}_\eta\right)_{i,j} = \phi_{i,j}\left(r^{-1}\right)\left(\lambda_\eta\right)_{i,j}$$

Time-Integration :

Using a four stage Runge-Kutta scheme, the systems of differential equations, Eqs.(1), are advanced in time. It can be written for the nth time level as

$$U^0 = U^n$$

$$U^1 = U^0 - \alpha_1.\Delta t.R\left(U^0\right) + \alpha_1.H^0.\Delta t$$

$$U^2 = U^0 - \alpha_2.\Delta t.R\left(U^1\right) + \alpha_2.H^0.\Delta t$$

$$U^3 = U^0 - \alpha_3 . \Delta t . R\left(U^2\right) + \alpha_3 . H^0 . \Delta t$$

$$U^4 = U^0 - \alpha_4 . \Delta t . R\left(U^3\right) + \alpha_4 . H^0 . \Delta t$$

$$U^{n+1} = U^4$$

where, at the $(q+1)$ st stage, we have

$$R\left(U^{q+1}\right) = \frac{1}{\Omega}\left[Q\left(U^q\right) - D\left(U^0\right)\right]$$

where, Ω is the volume of the cell being considered, $Q(U)$ is the discrete approximation of the convective and physical diffusive terms, and $D(U)$ denotes the artificial dissipation terms. Here,

$$\alpha_1 = 1/4, \ \alpha_2 = 1/3, \ \alpha_3 = 1/2, \alpha_4 = 1$$

Acceleration techniques

Three methods are employed to accelerate convergence of the basic explicit time-stepping scheme.

These techniques are as follows :

1.Local time stepping 2. Residual smoothing 3. Multigrid method

Local time stepping

For faster steady state calculation, the locally varying maximum allowable time step is used. In the present work the actual time step Δt is computed using

$$\Delta t = c_0 \left(\frac{\Delta t_c \cdot \Delta t_d}{\Delta t_c + \Delta t_d} \right)$$

where, Δt_c is the limit due to convective terms, Δt_d is the limit due to diffusive terms, and c_0 is a constant usually taken to be the Courant-Friedrichs-Lewy(CFL) number. In particular,

$$\Delta t_c = \frac{\Omega}{\lambda_\xi + \lambda_\eta} \qquad \text{where, } \Omega \text{ is the volume of a cell.}$$

$$\Delta t_d = \frac{\Omega^2}{K_t (\gamma \mu / \rho \, Pr) \left[|\bar{S}_\xi|^2 + |\bar{S}_\eta|^2 \right]}$$

where, λ_ξ and λ_η are defined in the equations of artificial dissipation, K_t is a constant that has been set equal to 2.5 based on numerical experiments.

Residual Smoothing

The stability range of the basic time stepping scheme can be extended using implicit smoothing of the residuals. For two-dimensional flows the residual smoothing can be applied in the form,

$$\left(1 - \beta_\xi \nabla_\xi \Delta_\xi \right) \left(1 - \beta_\eta \nabla_\eta \Delta_\eta \right) \bar{R}_{i,j} = R_{i,j}$$

where, $R_{i,j} = \dfrac{1}{\Omega}[Q(U) - D(U)]$ is original residuals for the explicit time-stepping scheme

and $\overline{R}_{i,j}$ represents the residuals after the sequence of smoothings in the ξ, η directions

with the variable coefficients β_ξ and β_η. The residual smoothing is applied in the second

and fourth time step of the four stage Runge-Kutta integration. In the equation, shown

above, it is necessary to solve a sequence of tri-diagonal equations for separate scalar

variables.

The expressions for variable coefficient β_ξ and β_η are written as

$$\beta_\xi = \max\left\{ \frac{1}{4}\left[\left(\frac{CFL}{CFL^*}\cdot\frac{\lambda_\xi}{\lambda_\xi + \lambda_\eta}\cdot\phi(r)\right)^2 - 1\right], \varepsilon\right\}$$

$$\beta_\eta = \max\left\{ \frac{1}{4}\left[\left(\frac{CFL}{CFL^*}\cdot\frac{\lambda_\eta}{\lambda_\eta + \lambda_\xi}\cdot\phi(r^{-1})\right)^2 - 1\right], \varepsilon\right\}$$

where, $\phi(r)$ and $\phi(r^{-1})$ are the same quantities defined for artificial dissipation, CFL is

the local courant number used in the computational scheme and CFL^* is the maximum

allowable local courant number based on stability analysis of the explicit Runge-Kutta

scheme. For the present computation, CFL is used as 3.5, whereas CFL^* as 2.5. The

quantity ε used in the equation above, is used as a limiter. Dimensional analysis carried

out found the value of ε lying between 0.10 and 0.25. Here, ε is used as 0.15.

Multigrid Method

The basic idea is to use coarser grids to speed up the propagation in the fine grid corrections. For the multigrid process, coarser meshes are obtained by eliminating every other mesh line in each coordinate direction.

In multigrid, the solution is initialized as,

$$U_{2h}^{(0)} = \frac{\sum U_h \Omega_h}{\Omega_{2h}}$$

where, the subscript refers to the mesh spacing value (2 and 4 for 2h and 4h respectively), and the sum is over the four fine grid cells that compose the 2h grid cell. This rule conserves mass, momentum and energy. On a coarse grid, a forcing function P is added to the governing discrete equations in order to impose the fine grid approximation. After the initialization of the coarse grid solution, this function is computed as follows :

$$P_{2h} = \Omega_{2h}^{-1} \sum \Omega_h R_h (U_h) - R_{2h} \left(U_{2h}^{(0)} \right)$$

Thus, the time-stepping scheme on the (m+1)st stage becomes,

$$U_{2h}^{(m+1)} = U_{2h}^0 - \alpha_{m+1} \cdot \Delta t \left[R_{2h} \left(U_{2h}^{(m)} \right) + P_{2h}^{(0)} \right]$$

This process is carried out on all coarser grids, and the corrections computed on each coarse grid are transferred back to the finer grid by linear interpolation. In the present work, a V-type cycle is used as a multigrid strategy. The process is advanced from the finer grid to the coarser grid without any intermediate interpolation, and when the coarser grid is reached, the correction is interpolated back to the finer grid. One Runge-Kutta step is performed on h-grid, two on 2h-grid and three in all other coarser grids. In the viscous flow calculations, the viscous terms are computed also on the coarser grids, while the

turbulent viscosity is evaluated only on the finest grid and then determined on each succeeding coarser grids by a simple averaging of surrounding finer grid values. Thus, the integrations of k and ε are performed only in the finer grids. The artificial dissipation model of the finest grid is replaced on the coarser grids with a simple constant coefficient second difference dissipation model. The multigrid strategy is illustrated in Fig-4.1.
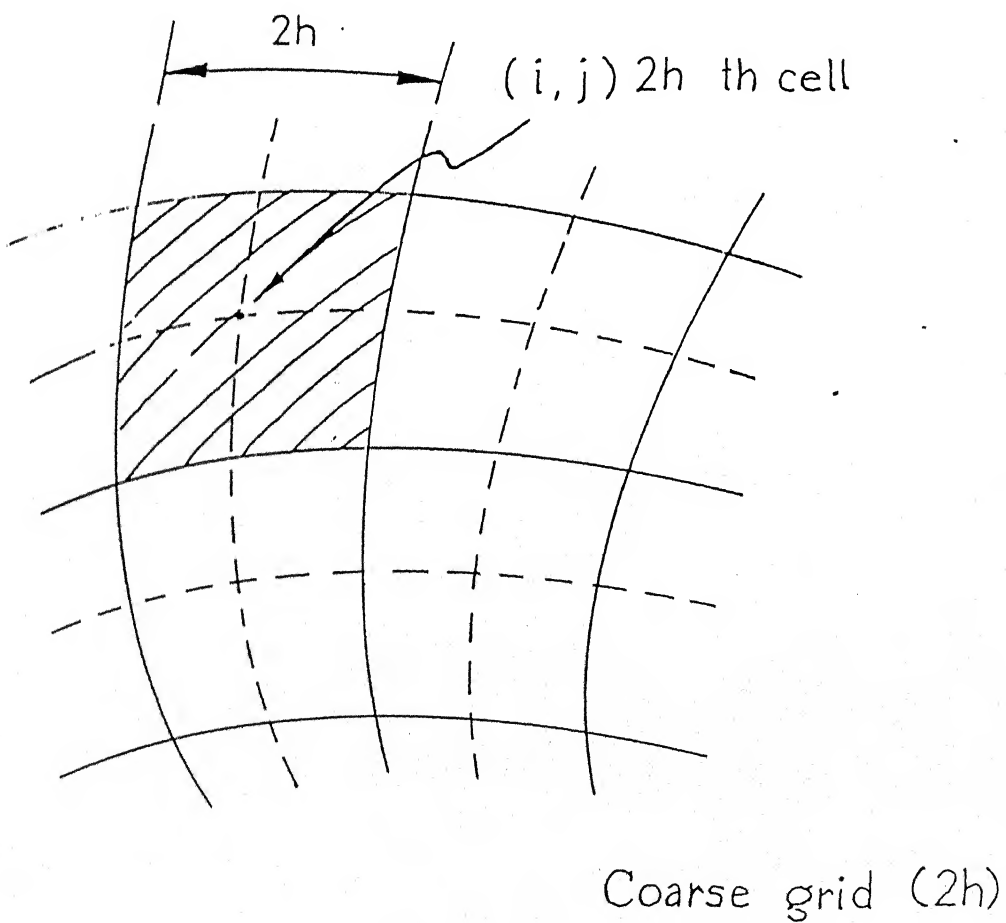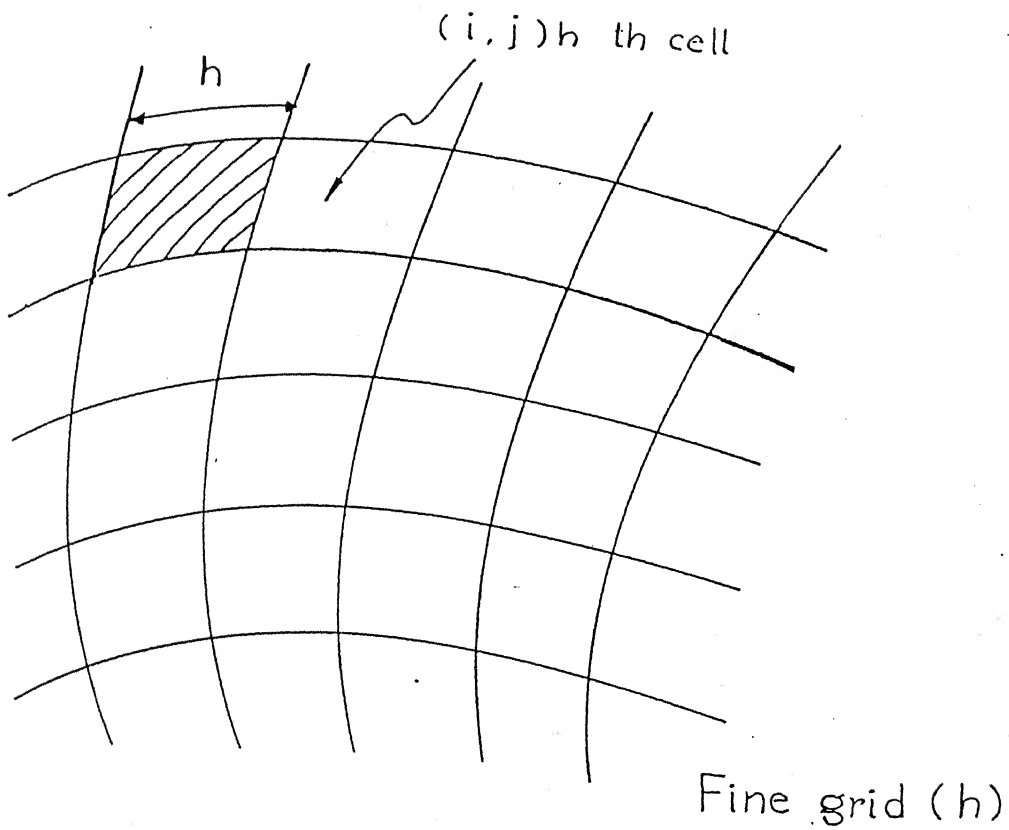
Fine grid (h)

Coarse grid (2h)

Fig. 4.1 Fine and Coarse grid used in Multigrid strategy.

CHAPTER-5

RESULTS AND DISCUSSION

5.1 Introduction

As mentioned in the literature review, it is very much essential to carry out a systematic analysis of flow and thermal field in turbomachinery blade passage under realistic conditions. The principal objective of the present study is to analyse the capability and efficiency of the low-Reynolds-number k-ε turbulence model due to Chien in predicting the complex transitional flow and heat transfer through turbomachinery blade passage for a wide range of exit Mach numbers, Reynolds numbers and free-stream turbulence intensities. Another objective is to compare the performance of k-ε Chien model with the k-ε Chien model modified with PTM(Production-Term-Modification) technique and to resolve the uncertainties possessed by turbulence models in predicting heat transfer in turbomachinery. The present analysis is restricted to the two-dimensional transonic turbine cascade flows. Comparisons of computed aerodynamics and convective heat transfer distributions are made with the published experimental data.

In the first section of this chapter, the simulation of transitional flow and the effects of Mach number, Reynolds number and free-stream turbulence level on the blade surface heat transfer of VKI turbine cascade are analysed. In the second section, predictions of transitional flow and heat transfer over Rolls-Royce rotor blade for a widely varying flow conditions are studied.

5.2 Two-dimensional Aero-thermal Analysis of Transonic VKI Turbine Cascade

In this section, the flow and thermal fields over a transonic VKI turbine cascade are presented. The test case is the VKI turbine blade [Art,1992] for which the experimental data of surface heat transfer and Mach number distribution were available for a wide range of flow conditions.

Grid generation and Boundary conditions :

The blade configuration and computational grid for the VKI turbine blade is shown in Fig-5.1. An algebraically generated H-grid is used for the blade-to-blade calculation. Axial grid distributions are chosen to give enough grid points to properly describe the shape of the blade blunt leading and trailing edges, and also to capture steep gradients of flow variables occurring at those regions. For the Navier-Stokes computation with low-Reynolds-number k-ε turbulence model, a highly refined exponentially stretched mesh spacing is employed in regions close to blade surface for resolving the viscous sub-layer
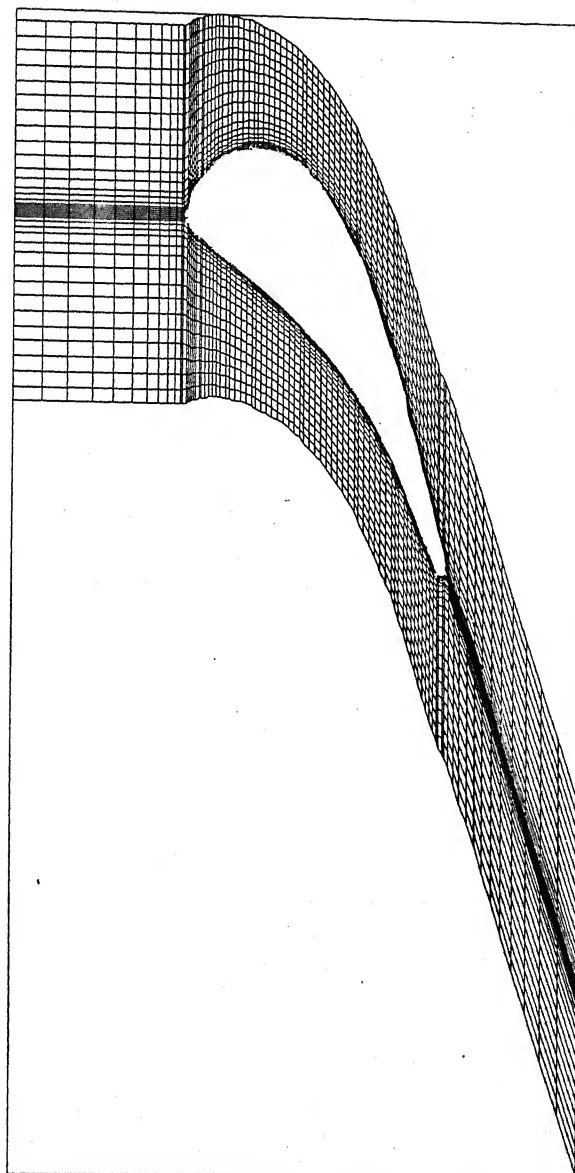
Fig. 5.1 Computational grid for VKI turbine cascade for Navier-Stokes Solution with LRN k-ε Chien model.

and a coarse uniform mesh spacing is used in the outer region. The first grid point above the wall is chosen so as to maintain the average y^+ of the order of unity.

The total pressure, total temperature and the flow angle are specified at the cascade inlet, and the axial component of the inlet velocity is computed as a part of the solution. The exit static pressure is imposed and all other variables are extrapolated from the interior. On the wall, no slip conditions are imposed for velocity, turbulent kinetic energy and dissipation rate along with vanishing normal temperature gradient or a constant wall temperature. The pressure at the blade surface is extrapolated from the interior. To simulate infinite blade row condition, a periodic boundary condition is enforced at the upstream and downstream of blades in a cascade. A constant values of k and ε are imposed at the inflow boundary based on the specified free-stream turbulence intensity and length scale as, $k_\infty = 1.5 Tu_\infty^2 V_\infty^2$ and $\varepsilon_\infty = c_\mu^{3/4} k_\infty^{3/2} / l_\infty$ where, l_∞ is assumed as 0.01 times the pitch of the blade passage.

In the present investigation, a grid sensitivity test reveals that a grid of 100×50 gives a grid independent solution for the engineering practice.

Blade velocity distribution :

The predicted isentropic Mach number distributions over the transonic VKI cascade are presented for the Navier-Stokes solution with the low-Reynolds-number k-ε turbulence model due to Chien in Fig-5.2. The predicted results are compared with the experimental

42

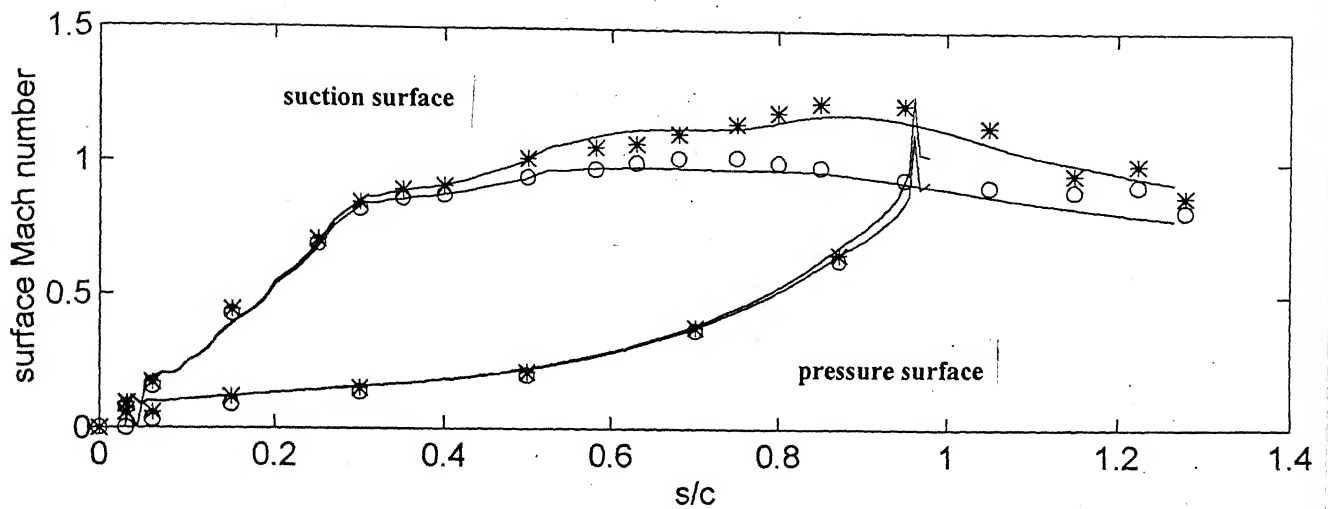| Experimental	Predicted	M_{2is}
oooo	———	0.875
****	———	1.02

Fig. 5.2 Comparison of Surface Mach number for VKI turbine cascade with experimental results [Arts, 1992] for the Navier-Stokes solution with LRN k-ε Chien model.

results for exit isentropic Mach numbers, $M_{2,is} = 0.875$ and $M_{2,is} = 1.02$ with

$Re_{2,is} = 1 \times 10^6$. The Reynolds number is defined based on the isentropic exit velocity

and the chord length. The experimental results indicate that the flow accelerates along the

suction surface up to s/c=0.3. A small plateau (s/c=0.35-0.4) is followed by

reacceleration. For the subsonic exit Mach number, the velocity variation is then rather

flat with a weak adverse pressure gradient starting from s/c=0.75. For transonic exit

Mach number, the flow accelerates up to s/c=0.95 and then a weak shock is observed at

s/c=1.05 on the suction surface. The velocity distribution along the pressure surface

varies smoothly from the leading to the trailing edge. It is evident from the figure, that the

predicted surface pressure distributions in both cases match extremely well with those of

experimental observations.

Blade heat transfer distribution :

Here, the comparisons of the predicted and the experimental results of convective heat

transfer distributions on the VKI blade for different Mach numbers, Reynolds numbers

and free stream turbulence intensities are presented. The blade convective heat transfer

strongly depends on the boundary layer transition. It is known that the transition on the

turbine blade surfaces is influenced by the free stream turbulence and the stream-wise

pressure gradient. Increasing free-stream turbulence promotes early transition, while

large flow acceleration tends to delay transition. The transition and consequently, blade

heat transfer distribution is also significantly influenced by the Reynolds number, the

Mach number, the shock wave location and its interaction with the boundary layer. Thus,

to obtain an accurate prediction of transitional flow and heat transfer, the effects of the above mentioned parameters must be resolved accurately on the behaviour of flows over a turbine blade.

The results are presented in the form of convective-heat transfer-coefficient $h\left(W/m^2k\right)$ versus non-dimensional length (s/c) measured along the suction and pressure sides from the theoretical stagnation point. All tests were performed for an upstream total temperature $T_{01} = 420\,K$ and a wall temperature of $T_w = 300\,K$.

The influence of exit Mach number on the blade heat transfer distribution for $Re_{2,is} = 10^6$ and $Tu_\infty = 4\%$ is presented in Fig-5.3. It shows that the predicted heat transfer distribution on the pressure surface matches well with the experimental results except very near to the leading edge, but on the suction surface heat transfer is over predicted due to the early prediction of the onset of transition for both the cases. The pressure surface boundary layer remains laminar. It should be noted that there is no significant influence of exit Mach number on the convective heat transfer distributions. The change of exit Mach number will not influence the surface heat transfer so long it does not change the boundary layer character.

The influence of free stream Reynolds number on the heat transfer distribution is illustrated in Fig-5.4 for $M_{2,is} = 0.92$ and $Tu_\infty = 4\%$. The Reynolds number has a very marked effect on the local variation of heat transfer. The heat transfer levels in both the laminar and turbulent regions are increased and the transition point moves forward as the

Reynolds number is increased. At the higher Reynolds number, the onset of transition on the suction surface is predicted too early with a rise in heat transfer values followed by a drop in heat transfer possibly due to large flow acceleration under favourable pressure gradient. The heat transfer has been over-predicted in the early part of the blade on the suction surface. The quality of prediction is improved for relatively low exit Re, although the onset of transition is predicted earlier as compared to the experimental observations. On the pressure surface, for higher Reynolds number, heat transfer is over-predicted in the early region of the blade surface and under-predicted in the later part. However, in both the suction and pressure surface, the overall predicted heat transfer increases with increase of Reynolds number as expected. In the stagnation region heat transfer is over-predicted.

The influence of free stream turbulence on the heat transfer distribution for $Re_{2,is} = 10^6$ and $M_{2,is} = 0.76$ is shown in Fig-5.5. On the suction surface, the Chien k-ε model predicts the transition onset too early for both free-stream turbulence intensities when compared to the experimental data. The predicted onset of transition is moved a small distance forward as Tu_∞ is increased from 4% to 6%. Thus, Chien model although mimic the behaviour of transition, it fails to predict properly the effect of Tu_∞ on the onset and length of transition. On the pressure surface, heat transfer is over-predicted in the early part of the blade and the flow remains in the laminar state.

From the above studies, it can be inferred that although the LRN k-ε model has been able to predict transitional flow, there exists a lot of discrepancies in the predicted level of

$$Re_{2,is} = 1 \times 10^6, \; T_{u\infty} = 4\%$$

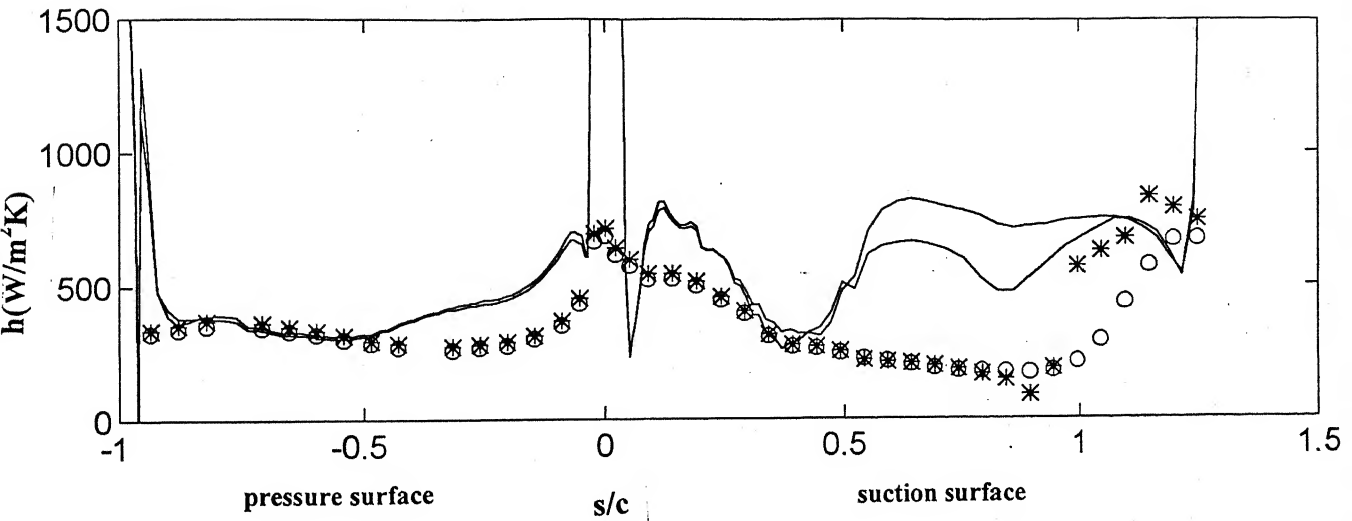| Experimental	Predicted	M_{2is}
oooo	————	0.76
****	————	0.92

Fig. 5.3 Effect of exit Mach number on surface heat transfer
for the VKI turbine cascade.

$M_{2,is} = 0.92$, $T_{u\infty} = 4\%$

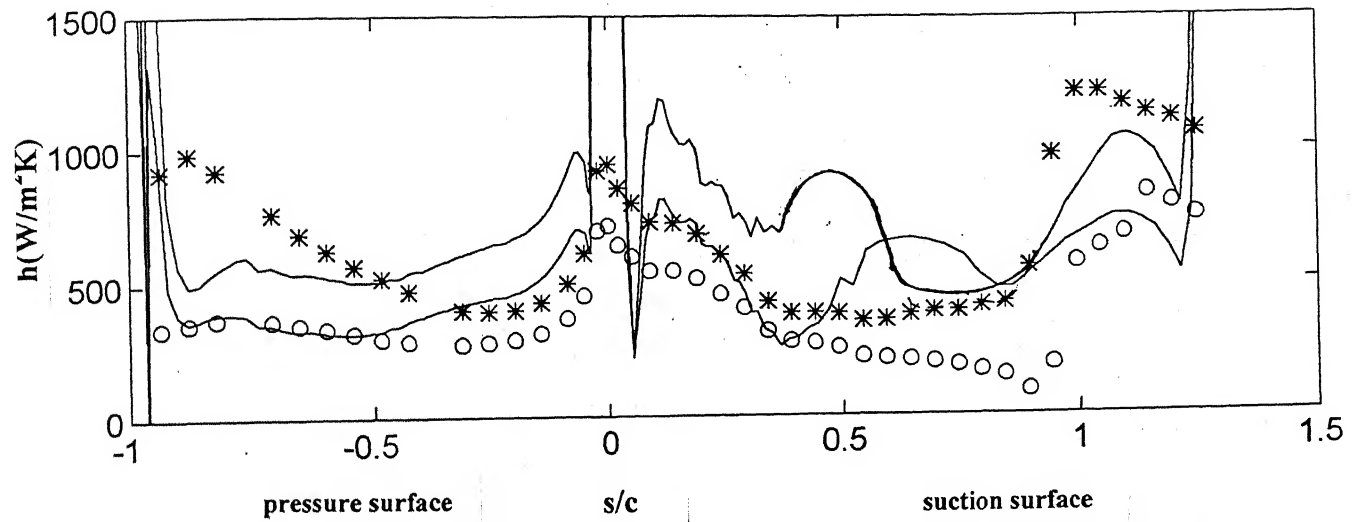| Experimental	Predicted	$Re_{2,is}$
0000	————	1×10^6
****	————	2×10^6

Fig. 5.4 Effect of Reynolds number on surface heat transfer
for the VKI turbine cascade.

$M_{2,is} = 0.76$, $Re_{2,is} = 1 \times 10^6$

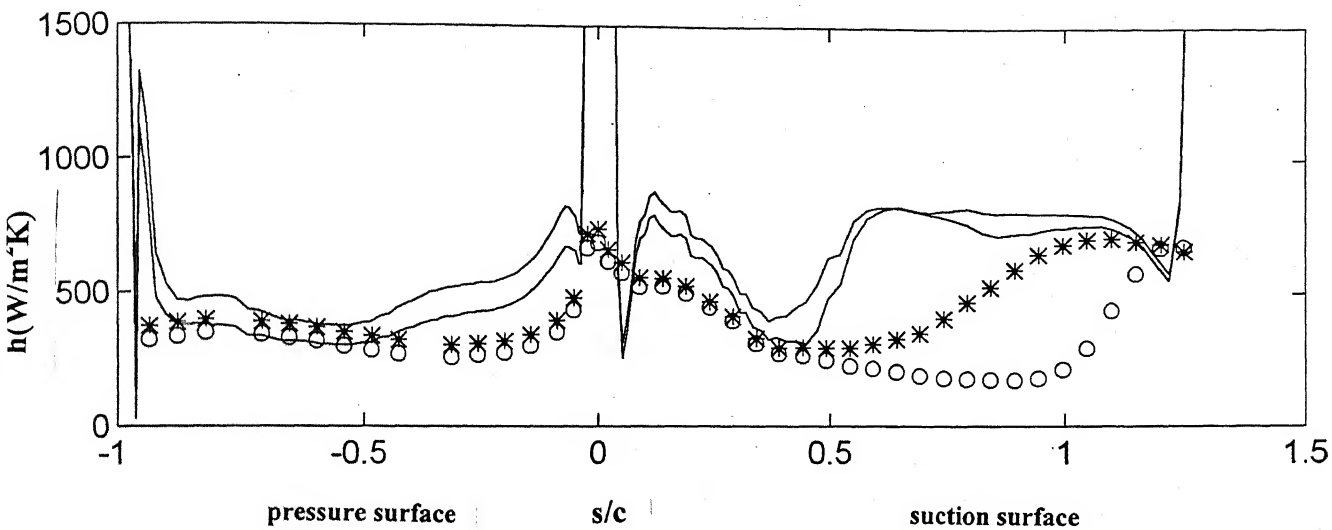| Experimental	Predicted	$T_{u\infty}$
˙ooo	————	4%
****	————	6%

Fig. 5.5 Effect of free-stream turbulence intensity on surface heat transfer for the VKI turbine cascade.

heat transfer and that of experimental values due to early detection of onset of transition with a sharp rise in heat transfer over a very short distance. In the following section, the heat transfer results are presented with kinetic energy Production-term-modification and compared with experimental observations.

Prediction with modified Chien model :

Fig-5.6 shows the comparison of LRN k-ε Chien model and modified Chien model in predicting the blade heat transfer for $Tu_\infty = 4\%, Re_{2,is} = 10^6$ and $M_{2,is} = 0.76$. The onset and length of transition on the suction surface are much better resolved by the modified Chien model when compared with the performance of Chien model. The level of heat transfer prediction and its trend match very well with the experimental results. However, still the onset of transition is predicted early even with PTM. On the pressure surface, the predictions by both model are nearly same and it compares moderately well with the experimental results. When Tu_∞ is increased to 6%, the performance of modified Chien model is depicted in Fig-5.7. Here also the modified Chien model tends to predict the onset of transition at the proper location on the suction surface and it captures the trend of experimental data. The modification improves dramatically the quality of prediction by properly resolving the influence of Tu_∞.

Fig-5.8 illustrates the improvement in prediction due to the modification invoked for $Re_{2,is} = 1 \times 10^6$, $Tu_\infty = 4\%$, $M_{2,is} = 0.92$. From the figure it is clear that Chien model predicts the onset of transition much early on the suction surface of the blade and the heat

$M_{2,is} = 0.76$, $Re_{2,is} = 1 \times 10^6$, $T_{u\infty} = 4\%$

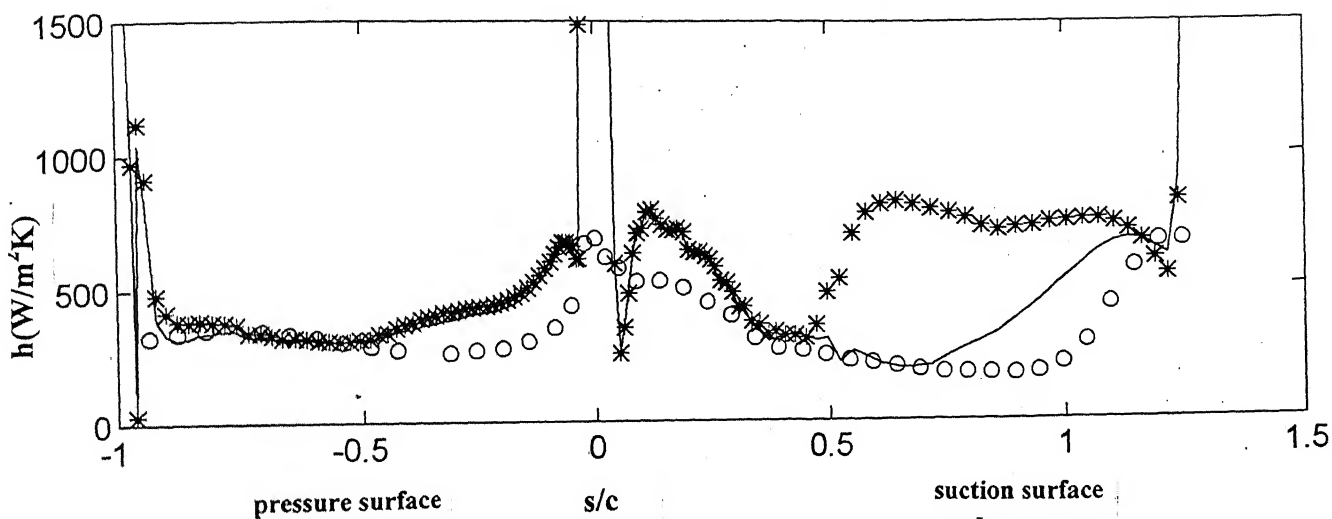| Chien model	Chien model with PTM	Experimental
*****	————	000000

Fig. 5.6 Surface heat transfer over VKI turbine cascade for 4% free-stream turbulence intensity: Chien model and Chien model with PTM.

$M_{2,is} = 0.76$, $Re_{2,is} = 1 \times 10^6$, $T_{u\infty} = 6\%$

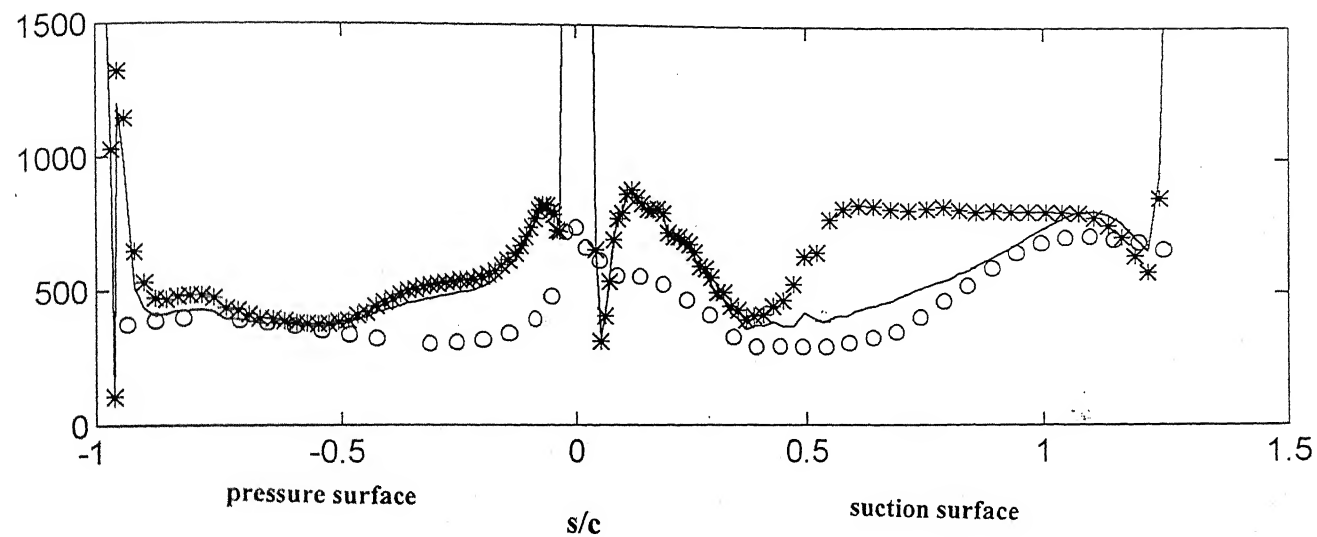| Chien model	Chien model with PTM	Experimental
*****	————	oooooooo

Fig. 5.7 Surface heat transfer over VKI turbine cascade for 6% free-
stream turbulence intensity: Chien model and Chien model with
PTM.

$M_{2,is} = 0.92$, $Re_{2,is} = 1 \times 10^6$, $T_{u\infty} = 4\%$

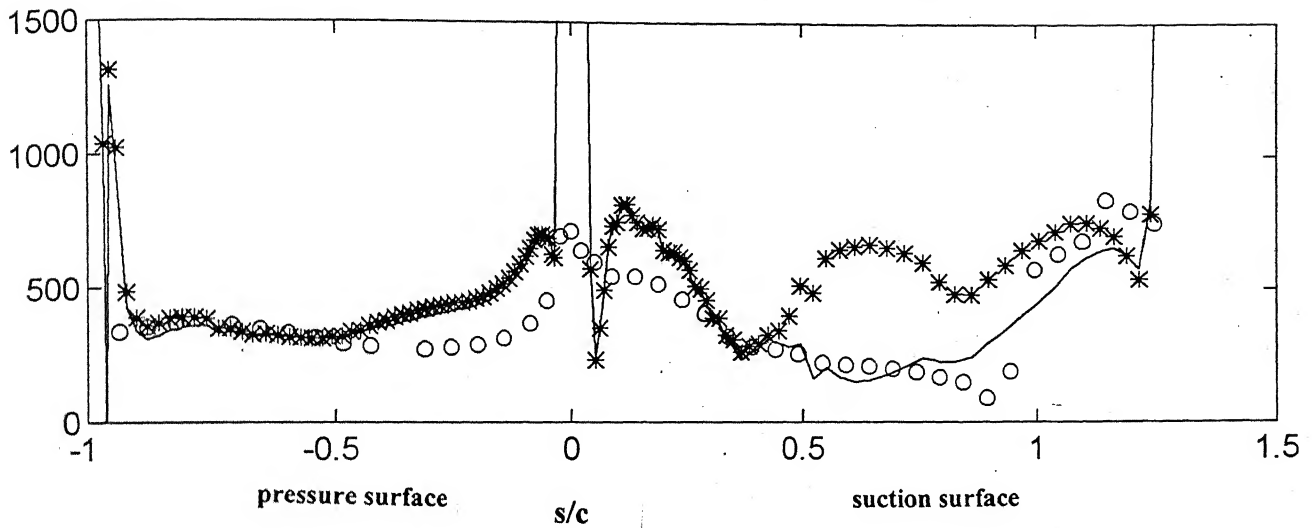| Chien model	Chien model with PTM	Experimental
✳ ✳ ✳ ✳	————————	o o o o o

Fig. 5.8 Surface heat transfer over VKI turbine cascade for low
Reynolds number: Chien model and Chien model with PTM.

transfer is over-predicted in the early part of the blade. The modified Chien model captures extremely well the trend of the convective heat transfer with proper estimation of onset and length of transition. Again on the pressure surface, the heat transfer predictions by both models are nearly same. In this particular case, the success of modification is extremely well felt. As the $Re_{2,is}$ is increased to 2×10^6, the comparison of Chien model and modified Chien model in predicting the blade heat transfer is shown in Fig-5.9. The dramatic improvement of predicted heat transfer distribution on the suction surface with modified Chien model can be well appreciated. In this case, the original Chien model fails to capture the trend of heat transfer distribution. However, on the pressure surface, no improvement is felt with the Production-term-modification.

5.3 Two-dimensional Aero-thermal Analysis of Transonic Rolls-Royce Turbine Rotor Blade

In this section, the aero-thermal analysis of low-solidity Rolls-Royce Turbine Rotor Blade is presented. The prediction of flow and heat transfer for different exit Mach numbers and Reynolds numbers are illustrated.

Grid generation and Boundary conditions :

The blade configuration and computational grid for the Rolls-Royce turbine blade is shown in Fig-5.10. An algebraically generated H-grid is used with 100×50 grid points.

$$M_{2,is} = 0.92, \ Re_{2,is} = 2 \times 10^6, \ T_{u\infty} = 4\%$$

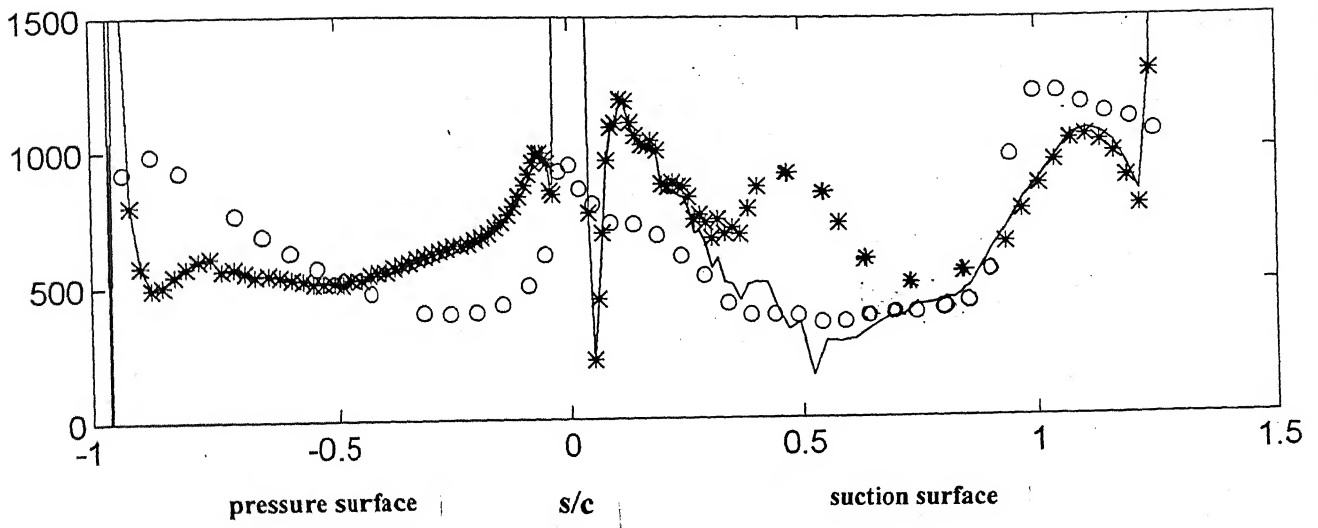| Chien model	Chien model with PTM	Experimental
*****	————	ooooo

Fig. 5.9 Surface heat transfer over VKI turbine cascade for high
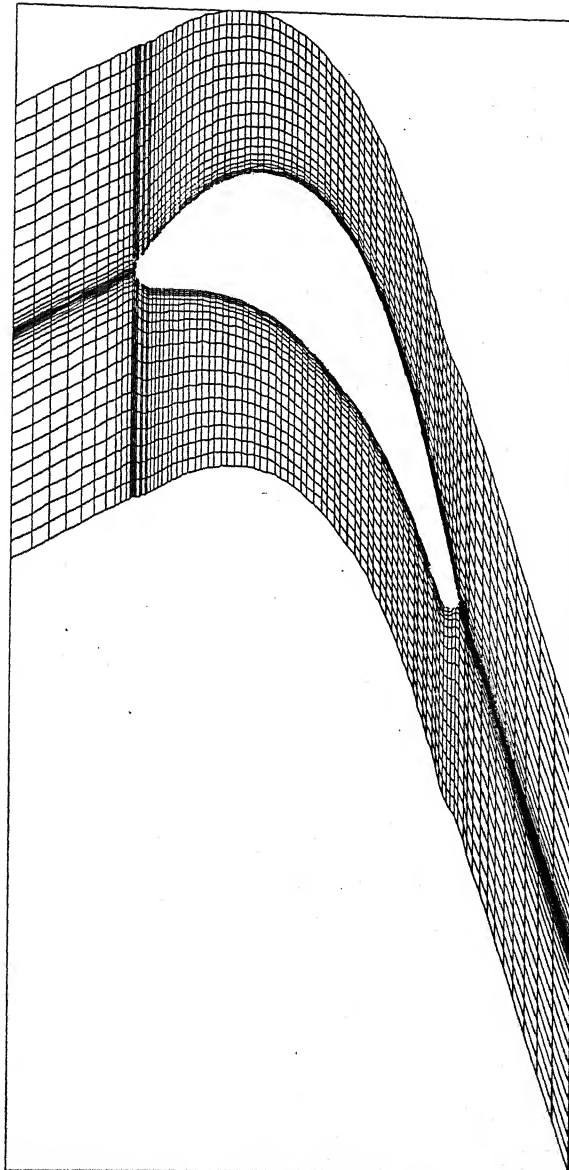Reynolds number: Chien model and Chien model with PTM.

Fig. 5.10 Computational grid for Rolls-Royce turbine rotor blade for Navier-Stokes Solution with LRN k-ε Chien model.

A highly refined exponentially stretched mesh spacing is employed in regions close to blade surface for resolving the viscous sub-layer. The boundary conditions are the same as already explained while presenting results on VKI guide vane.

The blade heat transfer is influenced by changes in exit Reynolds number, Mach number, and changes in the free-stream turbulence level; whereas, the pressure distribution is affected most significantly by changes in the flow exit Mach number. For these reasons, Nicholson et al [7] tested the Rolls-Royce turbine blade profile to measure the static pressure distribution at three exit Mach numbers $M_{2,is} = 0.78$, 0.96 and 1.1 for the design Reynolds number $Re_{2,is} = 1.113 \times 10^6$, while the heat transfer to the blade was measured with different combination of Reynolds numbers and Mach numbers at varying free stream turbulence levels. All tests were conducted for an upstream total temperature $T_{01} = 432K$ and a wall temperature $T_w = 288K$.

Blade Velocity Distribution :

The predicted surface Mach number distributions by Chien model for the Rolls-Royce turbine blade are presented in Fig-5.11 at the three exit Mach numbers and compared with experimental data [Nicholson.et.al,1984]. The experimental results indicate that at the design exit Mach number ($M_{2,is} = 0.78$), the suction surface flow has undergone a relatively strong acceleration up to 75 percent axial chord and then the flow is diffused. At an exit Mach number of 0.96, a peak suction Mach number of 1.25 is reached followed by a compression through a shock wave at approximately 85 percent axial

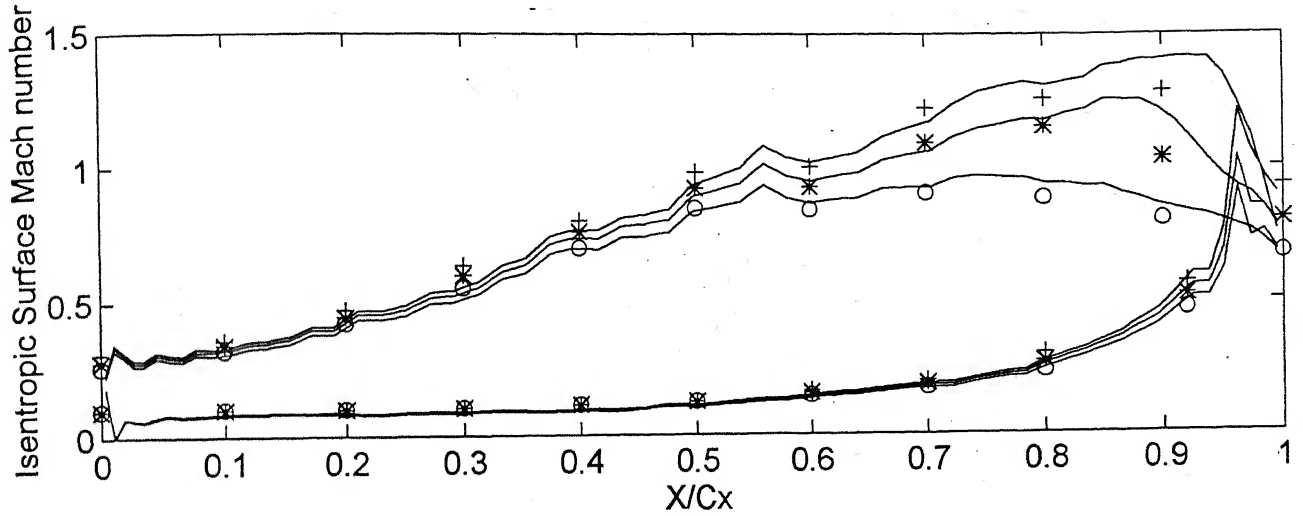| $M_{2,is}$	0.78	0.96	1.10
Experimental	Ooo	***	+++
Predicted	——	——	——

Fig. 5.11 Surface Mach number distributions for Rolls-Royce turbine blade : effect of exit Mach number.

chord. At the exit Mach number of 1.1, the peak suction Mach number rises to 1.4 followed by a shock wave compression at about 90 percent axial chord. For the pressure surface, Mach number is low till about 80 percent of the axial chord when the flow undergoes a rapid acceleration. As seen in Fig-5.11, the present calculation predicts the same trend of surface Mach number distributions for the three expansions ratios with fairly good estimation of the location of shock wave. Moreover, the solution has a tendency to slightly under-predict the suction surface Mach number in the frontal part (the first 50 percent of the axial chord) of the blade and over-predicted in the later part. The pressure surface is well resolved.

The predicted Mach number contour for the same blade is depicted in Fig-5.12 for $M_{2,is} = 1.10$, $Re_{2,is} = 1.113 \times 10^6$ and $Tu_\infty = 4\%$. This shows that the flow on the suction surface has undergone an initial acceleration and then compression occurs through a shock wave as detected near the rear part of the suction surface.

Blade Heat transfer Distribution :

The effect of Mach number variation on the heat transfer distributions for the Rolls-Royce turbine rotor blade is shown in Fig-5.13 for $Re_{2,is} = 1.113 \times 10^6$ and $Tu_\infty = 4\%$, where the LRN k-ε turbulence model due to Chien is used. Along the suction side, there is no change in the heat transfer rate in the laminar part of the boundary layer with a change in exit Mach number, and the predicted results also agree well with the experimental data in this region. In the turbulent region, there exist discrepancies of
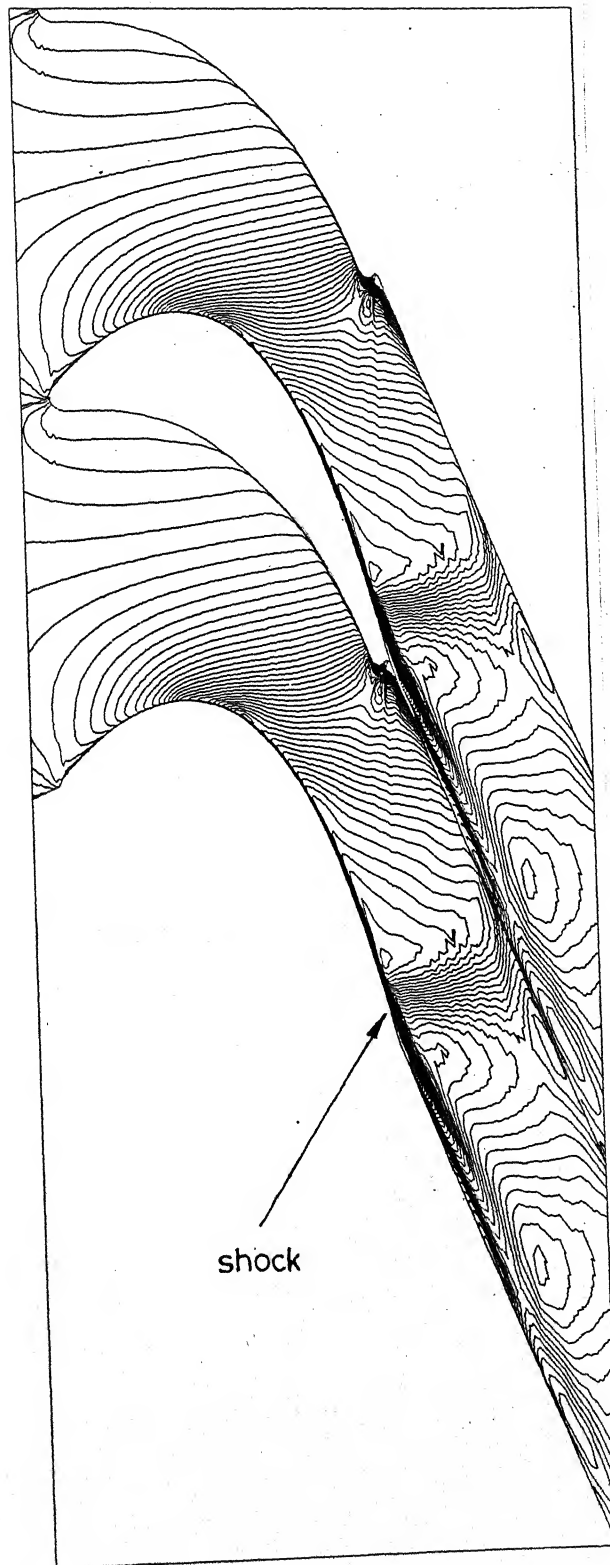
shock

Fig. 5.12 Predicted Mach number contours for flow over Rolls-Royce turbine blade for $M_{2,is}$=1.10.

$$Re_{2,is} = 1.113 \times 10^6, Tu_\infty = 4\%$$

$M_{2,is}$	0.78	0.96	1.10
Experimental	Ooo	***	+++
Predicted	——	——	——

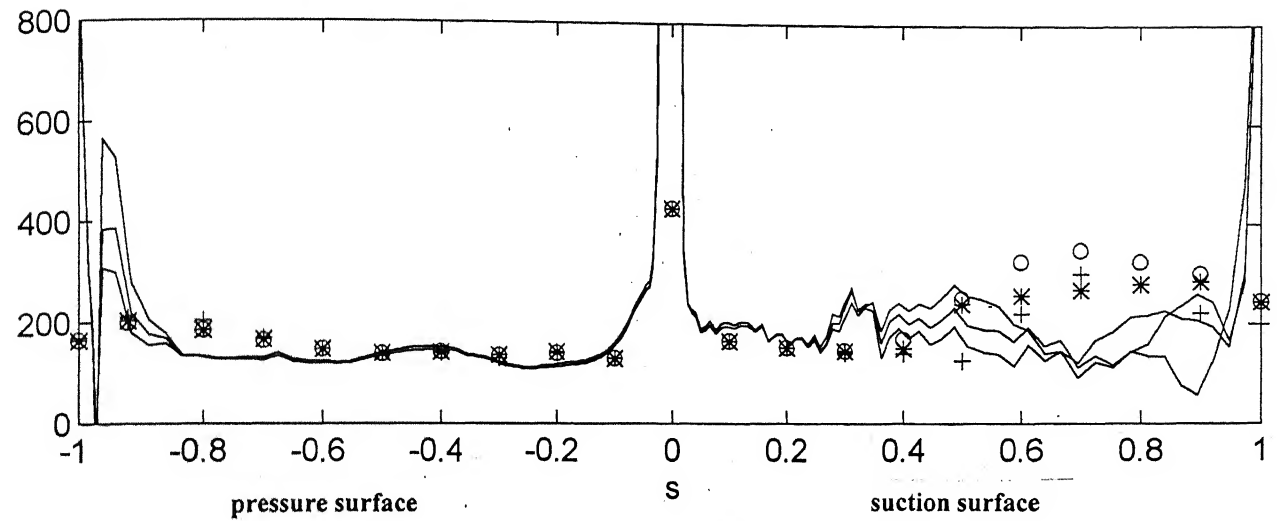pressure surface   s   suction surface

Fig. 5.13 Effect of exit Mach number on surface heat transfer for the Rolls-Royce turbine blade.

predicted heat transfer with that of experimental observations, the onset of transition is not well resolved and the heat transfer is under-predicted. Along the pressure side, the velocity distributions are almost similar for different exit Mach numbers. As a result, no significant difference appears in the predicted pressure side heat transfer distributions which agree well with the test results. The boundary layer on the pressure surface seems to remain laminar as obtained from the computed heat transfer result.

Fig-5.14 illustrates the effect of Reynolds number on surface heat transfer, where results from LRN k-ε Chien model are compared with experimental data. The experimental results show that heat transfer rate increases and transition point moves forward as the Reynolds number is increased on the suction surface. Chien model is able to predict fairly well the onset of transition and the trend of variation of heat transfer with exit Reynolds numbers. At the highest Reynolds number ($Re_{2,is} = 1.67 \times 10^6$), Chien model predicts slightly delayed transition followed by a sharp rise in the heat transfer. The surface heat transfer is under-predicted in the fully turbulent flow regime. On the pressure surface, the level of heat transfer is under-predicted in the later part of the blade and the boundary remains in the laminar state. Whereas, the experimental observation indicates a slow flow transition in that region. At the minimum Reynolds number, $Re_{2,is} = 0.557 \times 10^6$ the model detected an early transition on the suction surface. The pressure surface heat transfer level and trend are extremely well captured. At the design Reynolds number, $Re_{2,is} = 1.113 \times 10^6$, the onset of transition on the suction surface is well estimated by the present turbulence model, however, the fully turbulent region is slightly under-

$M_{2,is} = 0.78$, $Tu_\infty = 4\%$

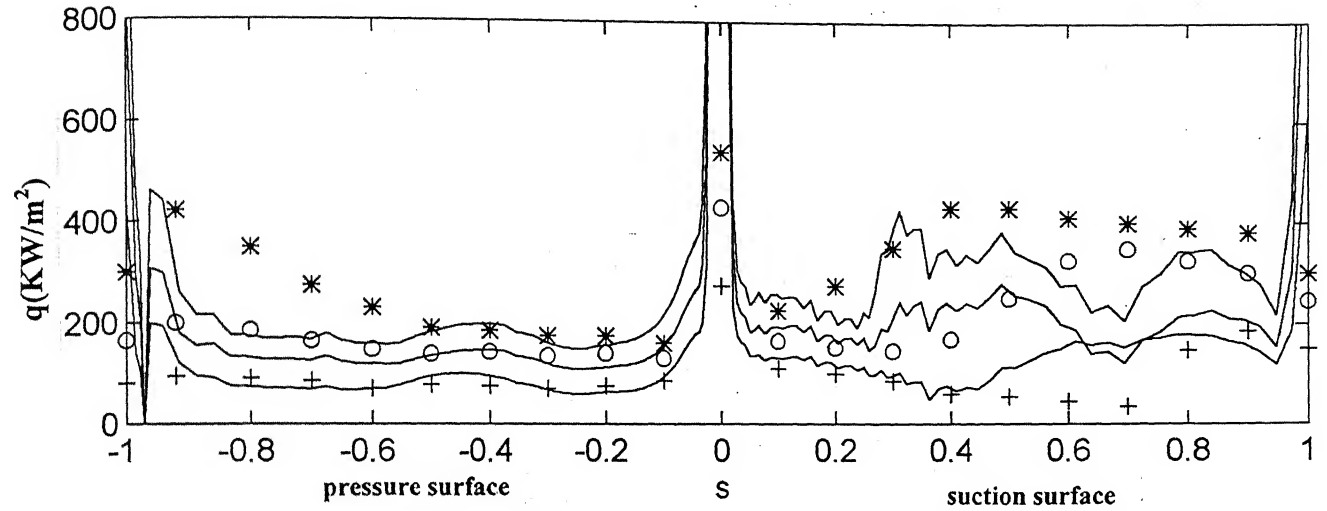| $Re_{2,is}$	0.557×10^6	1.113×10^6	1.670×10^6
Experimental	+++	ooo	****
Predicted	———	———	———

Fig. 5.14 Effect of Reynolds number on surface heat transfer for the
Rolls-Royce turbine blade.

predicted. The resolution in the pressure surface is extremely good. The boundary remains in the laminar state.

Performance of modified Chien model :

Figures 5.15 to 5.17 illustrate the performance of Chien model modified with Production-term-modification (PTM) technique in predicting flow and heat transfer over the rotor blade for different exit conditions.

Fig-5.15 shows the comparison of Chien model and the modified Chien model in estimating the blade heat transfer for $M_{2,is} = 0.78, Re_{2,is} = 1.113 \times 10^6$, $Tu_\infty = 4\%$ (design condition). On the suction surface, the location of onset of transition is better resolved, though the fully turbulent region is still under-predicted as that of Chien model. On the pressure surface, predictions of heat transfer by both model are same and it agrees well with the experimental result.

As already explained for low Reynolds number, $Re_{2,is}=0.557 \times 10^6$, an early transition is estimated by the Chien model resulting over-predicted heat transfer values in the fully turbulent region on the suction surface (Fig-5.16). The modified Chien model tends to shift the onset of transition downstream predicting heat transfer levels that match comparatively well with the experimental result. But in the last part of the blade on the suction side, the modified Chien model under-predicts the heat transfer. Here also predictions of heat transfer by both model are same on the pressure surface. As the exit

$M_{2,is} = 0.78$, $Re_{2,is} = 1.113 \times 10^6$, $T_{u\infty} = 4\%$

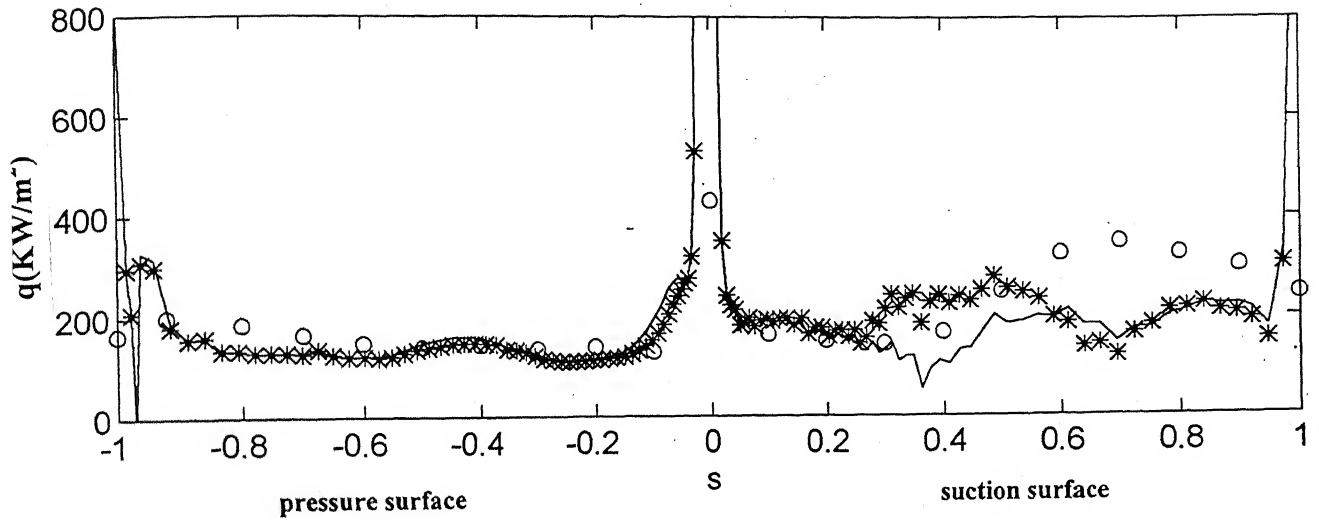| Chien model	Chien model with PTM	Experimental
*****	————	00000

Fig. 5.15 Surface heat transfer over Rolls-Royce turbine blade for
design condition : Chien model and Chien model with PTM.

$M_{2,is} = 0.78$, $Re_{2,is} = 0.557 \times 10^6$, $T_{u\infty} = 4\%$

Chien model	Chien model with PTM	Experimental
*****	————————	00000

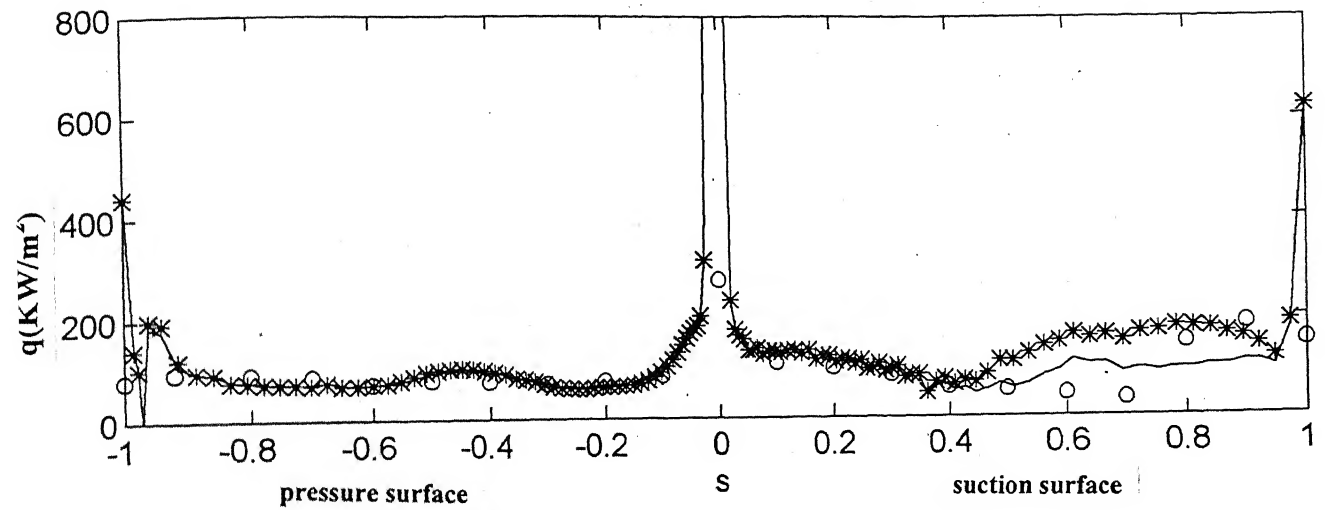

Fig. 5.16 Surface heat transfer over Rolls-Royce turbine blade for low
Reynolds number : Chien model and Chien model with PTM

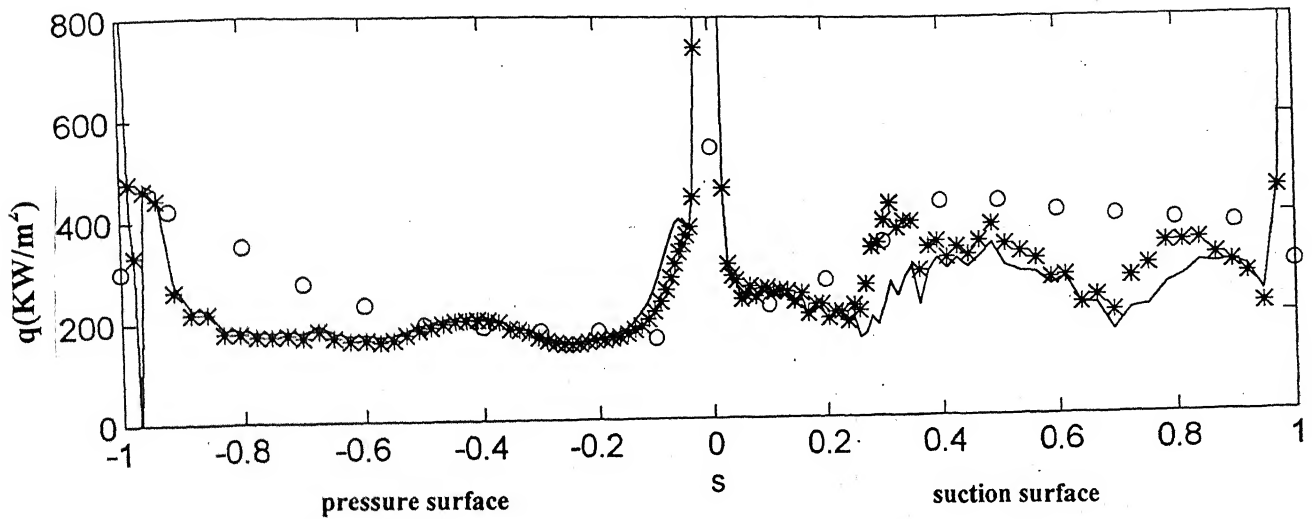| Chien model	Chien model with PTM	Experimental
*****	————	00000

Fig. 5.17 Surface heat transfer over Rolls-Royce turbine blade for high Reynolds number : Chien model and Chien model with PTM

Reynolds number is increased to $Re_{2,is}=1.67\times10^{6}$, the quality of prediction also remains the same with that of without PTM, although with the modification the length of transition resolved is more realistic.

From the overall predicted results of the surface heat transfer distributions on the VKI nozzle guide vane and the Rolls-Royce rotor blade, one can conclude that improvement in the quality of prediction by the kinetic energy Production-term-modification is well appreciated for the VKI blade. However, for the Rolls-Royce rotor blade, no such dramatic improvement is illustrated. This may be attributed by the fact that the heat transfer on the suction surface of the rotor blade is mainly governed by the onset of the laminar-turbulent transition. The process is controlled by the local values of pressure gradient and free-stream turbulence. However, the experimental data for the heat transfer distributions over the VKI blade exhibit more complex nature of boundary layer prevailing in a transitional state over a larger length of the blade. After the onset of transition, there occurs a delicate balance between the free stream turbulence and the pressure gradient effects, the former tending to promote and the later to retard the transition to a fully turbulent flow. This makes the boundary layer to stay in the transitional state for a longer time. The modified Chien model is able to resolve well the heat transfer predictions because of not only proper estimation of the onset of transition, but also the delicate balance of both the free stream turbulence and pressure gradient on the transition process and thus the transition length.

The complex nature of the boundary layer for the test cases over the VKI blade can be further illustrated by the surface pressure distributions under different flow conditions. Fig-5.2 demonstrates that initially flow accelerates along the suction surface under a favourable pressure gradient followed by a slow diffusion or re-acceleration. Free stream turbulence intensities are also changed along with exit Reynolds number and Mach number. However, for the Rolls-Royce blade, flow accelerates over almost the entire blade length followed by a recompression shock near the trailing edge (Fig-5.11). Hence boundary layer remains under favourable pressure gradient over almost full length of the blade. Here also for the test cases examined, the free stream turbulence is kept constant and only exit Reynolds number and Mach number are changed. This may probably explain the reasons why the heat transfer distributions on the suction surface of the Rolls-Royce blade is strongly governed by the onset of transition, whereas, the boundary layer on the VKI blade exhibits in a transitional state for a longer length. Thus, the delicate balance of opposing effects of pressure gradient and free stream turbulence on transition process is better reflected in the test cases over the VKI cascade depending on improved turbulence model to predict the behaviours.

CHAPTER-6

CONCLUSIONS

6.1 Conclusions :

The turbomachinery flows are among the most complex flows that encounter in engineering practice including laminar, transitional and turbulent flows; large pressure gradient and free stream turbulence; subsonic, transonic to supersonic flows etc. A reliable Navier-Stokes flow solver with an appropriate turbulence model is needed to resolve this complex flow.

The time-dependent, mass-averaged, two-dimensional, compressible Navier-Stokes equations are solved in the physical plane based on four-stage Runge-Kutta algorithm in finite volume formulation. Local time-stepping, variable-coefficient implicit residual smoothing and a full multigrid technique have been implemented to accelerate the convergence to the steady state solution. The artificial dissipation model used here is a blend of second and fourth order differences of the flow variables. Turbulence is simulated by the low-Reynolds-number version of the k-ε turbulence model due to Chien and also it has been modified with the Production-term-modification (PTM) technique to improve prediction in transitional region. The flow solver developed has been applied for the analyses of flow and thermal fields over two transonic turbine blades for a wide range of flow conditions.

The contribution of the present work is to implement the low-Reynolds-number version of two-equation turbulence model and particularly the modification of Production term in turbulent-kinetic-energy equation to control its growth-rate in the pre-turbulent region of boundary layer in a time-dependent general purpose Navier-Stokes solver, where conditions are less restrictive. Schmidt and Patankar [1991] proposed the modification and applied the same within the framework of boundary layer flow, where space-marching technique was used to solve the resulting parabolic equation. To limit the growth-rate of Production term, being proposed in analogy with reaction theory, a time scale was used. The time scale was related to the local velocity. However, for the present analysis, in a framework of hyperbolic system using unsteady Navier-Stokes equations, the local production of turbulent kinetic energy term (P_k) is allowed to grow naturally and while applying the modification, the time scale is considered to be of the order of local time step fixed from the stability theory of the scheme. An intuitive guess drives the investigation to fix the P_k value at a particular location considering also the upstream effects by some relaxation, which results an improved predictions of the transition region location and length. This may be physically related to the fact that the boundary layer character and flow transition are highly influenced by the upstream flow history.

The overall prediction of the surface Mach number and the heat transfer distributions for a widely varying flow conditions indicate that the unmodified k-ε LRN model has simulated the effects of Reynolds number and Mach number on the heat transfer distributions with accuracy that is acceptable for engineering application. Some remarkable discrepancies between the computed and the experimental results appear in

predicting the onset and length of transition. Particularly, it fails to correctly simulate the opposite effects of the free-stream turbulence and pressure gradients in the transition process in many situations. This results in an early onset of the laminar-turbulent transition with a short transitional length causing a sharp rise of surface properties. The modified Chien model as applied to the time-dependent Navier-Stokes flow solver is shown to overcome many of the shortcomings as stated indicating a consistent and improved prediction of the transition location and length for a widely varying flow conditions.

6.2 Suggestions for Future work :

The present two-dimensional Navier-Stokes code with two-equation turbulence model can be extended to three-dimensional for the realistic simulation of turbomachinery flow in a more efficient manner. One can also include the effects of rotation for the analysis of flow in rotating blades. The code can be used for the simulation of unsteady flows also if a duel time-stepping algorithm can be incorporated.

In the present code, the turbulence has been simulated using low-Reynolds-number k-ε turbulence model due to Chien with a modification due to Schmidt and Patankar. The other low-Reynolds-number k-ε turbulence models such as Lam-Bremhorst model, Launder-Sharma model, Fan-Lakshminarayana-Barnett model etc can be used and compared with the Chien model in evaluating the performance of different models in predicting the transitional flow and heat transfer in turbomachinery blade passage.

REFERENCES

1.A. Arnone and R. C. Swanson, "A Navier-Stokes Solver for Turbomachinery Applications", **Journal of Turbomachinery**, Vol. 115,pp. 305-313, 1993.

2.C. K. G. Lam and K. Bremhorst, "A modified form of the k-ε Model for predicting Wall Turbulence", **Journal of Fluids Engineering,** Vol. 103,pp. 456-460, 1981.

3.D. Biswas and Y. Fukuyama, "Calculation of Transitional Boundary Layers with an improved Low-Reynolds-Number version of the k-ε Turbulence Model", **Journal of Turbomachinery,** Vol. 116,pp. 765-773, 1994.

4.Debashis Basu, "Development of a Three Dimensional Navier-Stokes Solver with Multigrid Algorithm for Turbomachinery Applications", **M-Tech Dissertation, Department of Mechanical Engineering, I.I.T Kanpur, 1999**

5.G. A. Gerolymos, "Implicit Multiple-Grid Solution of the Compressible Navier-Stokes Equations Using k-ε Turbulence Closure", **AIAA Journal**, Vol. 28, No. 10,pp. 1707-1717, 1990.

6.J. Luo and B. Lakshminarayana, "Numerical Simulation of Turbine Blade Boundary Layer and Heat Transfer and Assessment of Turbulence Models", **Journal of Turbomachinery**, Vol. 119,pp. 794-801, 1997.

7.J. H. Nicholson, A. E. Forest, M. L. G. Oldfield and D. L. Schultz, "Heat Transfer optimized Turbine Rotor Blades-An Experimental study using Transient Techniques", **Journal of Engineering for Gas turbines and Power,** Vol. 106, pp. 173-182, 1984.

8.K. Chien, "Prediction of Channel and Boundary-Layer Flows with a Low-Reynolds Number Turbulence Model", **AIAA Journal**, Vol. 20, pp. 33-38, 1982.

9.M. Koiro and B. Lakshminarayana, "Simulation and Validation of Mach Number Effects on Secondary Flow in a Transonic Cascade Using a Multigrid, k-ε solver", **Journal of Turbomachinery**, Vol. 120,pp. 285-297, 1998.

10.M. G. Turner and I. K. Jennions, "An Investigation of Turbulence Modeling in Transonic Fans including a novel implementation of an implicit k-ε Turbulence Model", **Journal of Turbomachinery**, Vol. 115,pp. 249-260, 1993.

11.Robert F.Kunz and Budugur Lakshminarayana, "Explicit Navier-Stokes Computation of Cascade Flows Using the k-ε Turbulence Model", **AIAA Journal,** Vol. 30,No. 1,pp. 13-22, 1992.

12. R. F. Kunz and B. Lakshminarayana, "Three-Dimensional Navier-Stokes Computation of Turbomachinery Flows Using an Explicit Numerical Procedure and a Coupled k-ε Turbulence Model", **Journal of Turbomachinery**, Vol. 114, pp. 627-642, 1992.

13. Ridha Abid, "Evaluation of Two-Equation Turbulence Models for predicting Transitional Flows", **International Journal of Engineering Science,** Vol. 3, pp. 831-840, 1993.

14. R. C. Schmidt and S. V. Patankar, "Simulating Boundary Layer Transition with Low-Reynolds-Number k-ε Turbulence Models: Part 1-An evaluation of Prediction Characteristics", **Journal of Turbomachinery,** Vol. 113, pp. 10-17, 1991.

15. R. C. Schmidt and S. V. Patankar, "Simulating Boundary Layer Transition with Low-Reynolds-Number k-ε Turbulence Models: Part 2-An Approach to improving the Predictions", **Journal of Turbomachinery,** Vol. 113, pp. 18-26, 1991.

16. S. Sarkar and T. K. Bose, "Comparison of different Turbulence Models for Prediction of Slot-Film cooling: Flow and Temperature Field", **Numerical Heat Transfer,** Part B, 28:217-238, 1995.

17. Sarkar S. "Prediction of Transitional Flow and Heat Transfer over Transonic Turbine Cascades", **Proceedings of the NCABE 96,** December 28-30, 1996.

18. V. Michelassi, F. Martelli, R. Denos, T. Arts, C. H. Sieverding, "Unsteady Heat Transfer in Stator-Rotor interaction by Two-Equation Turbulence Model", **Journal of Turbomachinery,** Vol. 121, pp. 436-447, 1999.

19. W. Rodi and G. Scheuerer, "Scrutinizing the k-ε Turbulence Model Under Adverse Pressure Gradient Conditions", **Journal of Fluids Engineering,** Vol. 108, pp. 174-179, 1986.

20. W. P. Jones and B. E. Launder, "The Calculation of Low-Reynolds-Number phenomena with a Two-Equation Model of Turbulence", **International Journal of Heat and Mass Transfer,** Vol. 16, pp. 1119-1130, 1972.